

POLITECNICO DI TORINO

Laurea magistrale
in Nanotechnologies for ICTs

Master Thesis

Sensor integration and integrated flow control within microfluidic POC devices



Relatore

prof. Matteo Cocuzza

Corelatore

Prof. Carlo Ricciardi

Candidato

Giacomo Di Dio

Anno accademico 2019-2020

Abstract

Background: This master thesis presents the work and the experiments performed at Micronit micro technologies in the framework of the KardiaTool project. Micronit is a company headquartered in Enschede, Netherlands, specialized in the design, development and production of state-of-the-art devices for microfluidics and MEMS applications. The company offers a wide range of services and products, such as organ-on-chip, microreactors and micromixers design, development, prototyping and manufacturing. The aim of the KardiaTool project is to integrate the concept of saliva biosensing into clinical practicing for addressing the medical needs in personalized heart failure diagnosis and therapy monitoring at point of care. The KardiaTool platform will be a complex system, incorporating mechanical, electrical and microfluidic subsystems and the different interfaces that link them. The main innovation presented by KardiaTool consists in the incorporation of four saliva biomarkers already proven in laboratory setting into a device that will be used at the point of care and will be accessible to different medical structures and usable by medical professionals. The different biomarkers will be sensed through the magnetic sensing of functionalized magnetic nanoparticles. The choice of saliva as source of biomarkers is forecasted to be beneficial for the healthcare community due to being cost effective, non-invasive, more convenient and acceptable for both patient and healthcare operators in comparison to more common biological matrix like blood.

Objectives: This thesis will report the work performed on two different aspects of the KardiaTool platform: The first part of the working process was focused on the integration of the silicon chip for sensing into a polymeric cartridge through hybrid bonding; the second part was focused on the design, fabrication and characterization of the microfluidic polymeric cartridge present in the Lab-on-chip part of the device.

Methods: For the sensor integration part of the work four different glues were testes and dispensed on polymeric dummy chips prepared for the occasion. The parameters affecting the dispensing process were optimized until a homogeneous deposition of glue was obtained. The chips were then bonded with glass slides and the quality of the bonding was assessed. For the polymeric chip cartridge characterization, the polymeric valves and the polymeric channels were characterized. The liquid flow rate and stability of the different batch of chips were measured, and the quality and the behaviour of the valve was observed through fluorescence microscopy. The complete working routine of the chip was tested, and the sequence optimized.

Conclusions: Regarding the sensor integration, the obtained results were positive, and it was demonstrated to be possible to dispense precisely different kind of glue in order to obtain a uniform, hermetic bonding between a silicon chip and the polymeric cartridge. Set of optimized parameters for an optimal bonding were obtained. Regarding the chip characterization, the behaviour of different batches of chips was analysed and the design and the fabrication of the sample was improved through the internship, ending with a functioning prototype for future experiments.

List of abbreviation

HF: Heart failure

POC: Point of care

MNBS: Micro Nano Bio System

LOC: Lab on chip

MNPs: Magnetic nanoparticles

ISFET: Ion sensitive field effect transistor

GLP: Good Laboratory Practice

GMP: Good Manufacturing Practice

GCP: Good clinical Practice

PCB: Printed circuit board

NO: Normally open valve

NC: Normally closed valve

PS: Polystyrene

ISFET: Ion sensitive field effect transistor

List of images

Figure 1. Main concepts of KardiaTool Project [1]	12
Figure 2. KardiaTool high level architecture	14
Figure 3. Working steps for KardiaTool functioning	14
Figure 4. Schematization of KardiaTool fluidic system	18
Figure 5. Magnetic particles with captured biomarkers fixed to the coils	20
Figure 6. Bonding of the magnetic particles into the functionalized surface of the biosensor	20
Figure 7. LOC and POC diagram description	22
Figure 8. LOC schematic	22
Figure 9. Schematic representation of the microfluidic system integrated in the disposable LOC ..	23
Figure 10. A prototype of the microfluidic cartridge	26
Figure 11. Schematic of the fluidic network and description of the steps needed to perform the KardiaTool assay in the LOC. The components of the microfluidic system are highlighted, such as the valves and the chip chambers.....	27
Figure 12. Microfluidic cartridge prototype design: A) 3D isometric view of the cartridge prototype. B) 3D exploded view showing the 5 layers composing the cartridge. C) View from the chamber side and description of the different elements.....	28
Figure 13. Layout and numbering of the microfluidic valves in the chip	30
Figure 14. Process flow for the fabrication of the thermoplastic disposable cartridge prototypes. 31	
Figure 15. front view of the polymeric cartridge	31
Figure 16. Reservoir prototyping. A) Schematic of the cross section of the reservoir mounted on the microfluidic cartridge. B) Picture of the reservoirs assembled on the fluidic cartridge and filled with a blue-stained liquid.....	32
Figure 17. A) Microfluidic valve component design cross section [22] . B). exploded and assembled view of a valve[22]	34
Figure 18. Image of V11, V12 and V13, forming the internal peristaltic pump.....	35
Figure 19. Working routine of the peristaltic pump	35
Figure 20. ISFET biosensor [1]	41
Figure 21. Design of the ISFET device integrated in the KardiaLOC	41
Figure 22. Magnetic incubator chamber designed for the handling of biomarkers attached to the MNPs	43

Figure 23. Single coil design and array of coils	44
Figure 24. cross section of the assembled Lab-on-chip.....	46
Figure 25. Schematic of the polymeric cartridge with the ISFET chamber (on the right) and the magnetic chamber (on the left) highlighted in red.....	47
Figure 26. Dummy polymeric chip cartridge.....	48
Figure 27. DD-500 dispensing machine	49
Figure 28. Results of NOA68 glue dispensing. A) dispensing of the glue with non-optimized parameters, overflow and non-uniform distribution of glue are present. B) distribution of glue with optimized parameters. Is possible to notice that the glue is not perfectly uniform. C) distribution of glue with definitive parameters.....	54
Figure 29. Dummy chip after the processes of deposition and bonding with a piece of glass slide.	55
Figure 30: Results of Dymax glue dispensing. A) dispensing of the glue with non-optimized parameters, huge overflow is present due to the low viscosity of the glue. B) distribution of glue with optimized parameters. Is possible to notice that the glue is not perfectly uniform. C) distribution of glue with definitive parameters.....	56
Figure 31. Dispensing results obtained with Permabond glue with parameters adjusted from previous experiments. The deposition is acceptable with non-optimized parameters even in the glue is not homogeneous since there is no strong overflow.....	57
Figure 32. IQ-BOND 9419 UV glue test dispensing.....	57
Figure 33. NOA68 bonding fluorescence test result. A) The fluorescent dye does not leak through the bonding connections, and completely fills the chamber. B) Same instance as in figure A), but some air is trapped inside the chamber. The bonding is still hermetic.....	59
Figure 34. Pictures of an example of a test sequence for validating a valve functionality.	61
Figure 35. Valve observed through optical microscopy. 32.a) Valve in open state; 32.b) Valve in closed state	62
Figure 36. Observation of valves through fluorescence microscopy: 33.a) valve in idle state, 33.b) valve in open state, 33.c) valve in closed state.....	63
Figure 37. Modification of image parameters of figure 33 through the software IMAGEJ.....	64
Figure 38. images of a functional and a dysfunctional valve. 3.a) presents a fully functional valve in closed state; 3.b) presents a malfunctioning valve and is possible to observe leaks through the pneumatic seal.....	65

Figure 39. observation of a blocked valve from the third chip batch. In this valve, the membrane does not deflect independently from the pressure that is applied.....	66
Figure 40. Membrane in plastic state, with presence of corrugations in the material	67
Figure 41. Fully functional valve with imperfect bonding at the edge of the membrane.....	67
Figure 42. Use of the ImageJ software for the 2D analysis of the behavior of a membrane. The brightness of the pixels is extracted along a path (in yellow) and plotted	68
Figure 43. Results of 3D visualization based on the analysis of the brightness of the pixels. A) Valve in idle state. B) Valve in open state. C) Valve in closed state	69
Figure 44. Flow rate characterization for the three analyzed chips	71
Figure 45. Flow stability characterization for the three analyzed chips.....	72
Figure 46. Characterization of the flow stability with and without MNPs.	73
Figure 47. Microscope images of the micropump valves when pumping the MNPs solution from a sample reservoir to the waste reservoir. A) Pictures of each pump valves once the MNPs solution has just passed the micropump. B) Pictures of each pump valves after pumping 4 mL of the MNPs solution.	74
Figure 48. a) Filling of the magnetic chamber; b) Filling of the ISFET chamber through the magnetic chamber; c) Filling of the buffer to ISFET chamber line.	75
Figure 49. sample 1 processing.....	76
Figure 50. sample 2 processing.....	76
Figure 51. Sample 3 processing.....	77
Figure 52. sample 4 processing.....	77
Figure 53. Buffer flowing to the waste without passing through the magnetic chamber	78
Figure 54. Testing of the backflow sequence for the priming of the system. A) Buffer is pumped from the waste tank to the buffer tank through the ISFET chamber. B) Buffer is pumped through the magnetic chamber. C) Buffer is pumped through the tanks outlet.....	80
Figure 55. Unsuccessful priming attempt, with internal bubbles still present.....	81

Summary

1. The KardiaTool project: concept and approach.....	10
1.1. KardiaTool general architecture	13
2. KardiaTool working assay description	16
2.1. Biomarkers for HF detection	16
2.2. Biomarker measurement procedure	17
2.3. Pre-measurement procedure	19
2.4. Single measurement and complete measurement procedure	19
3. KardiaTool LOC/POC design and specification.....	21
4. KardiaTool components description	25
4.1. Microfluidic cartridge	25
4.2. Fabrication of the microfluidic cartridge	30
4.3. Reservoir prototypes	32
4.4. Microfluidic Valves working principles and functionality.....	33
4.5. Integrated microfluidic pump.....	34
4.6. Functionalized magnetic nanoparticle	37
4.7. ISFET immunosensors	39
4.8. Electromagnetic chamber and Magnetic coils	42
5. Sensor integration.....	45
5.1. Theory and framework	45
5.2. Materials and equipment	47
5.3. Dispensing test parameters.....	51
5.4. Optimization of the parameters for the deposition of a single glue.....	53
5.5. Optimization of parameters for glues with different characteristics.....	55
5.6. Bonding strength and hermeticity tests results	58
5.7. Considerations on the testing results.....	59
6. Microfluidic chip testing and characterization	60
6.1. Introduction and methods.....	60
6.2. Microfluidic valves characterization.....	61
6.2.1. Valve operation.....	61
6.2.2. optical characterization of the microfluidic valves.....	62

6.2.3. Fluorescence testing	63
.....	68
6.3. Characterization procedure	70
6.4. Magnetic nanoparticles testing	73
6.5. Testing of the working assay	75
6.6. Priming optimization	78
7. Conclusions and next steps.....	82
8. Bibliography	84

1. The KardiaTool project: concept and approach

The KardiaTool is a research project developed within the Micronit microtechnology company. Micronit is a company headquartered in Enschede, Netherlands, specialized in the design, development and production of state-of-the-art devices for microfluidics and MEMS applications. Within the main compound of the company a clean room structure is present, where is possible to perform processes such as lithography, etching, micromachining, assembly and wafer bonding. Micronit offers a wide range of services and products related to Lab-on-chips and MEMS, ranging from developing organ-on-chip and microreactors to research products and prototyping services.

“The aim of the KardiaTool project is to translate a laboratory proven concept of a saliva biosensor to the clinical practice for addressing the priority needs in personalized cardiovascular diseases diagnosis and therapy monitoring at the point of care.”[1].

Cardiovascular diseases, a term that covers a wide group of medical problems that affect the circulatory system, are one of the leading causes of death in EU. According to Eurostat, in 2016 just over 1.9 million people from EU-28 died from diseases of the circulatory system, which was equivalent to 36.7% of all deaths [2]. These diseases also bear a considerable impact both on the government budget for healthcare and on the quality of life of the patients and their families, forcing re-hospitalization and increasing mortality and morbidity. In Europe, the cost related to HF treatment account for approximately 2% of the total healthcare cost, the most of it consisting in the cost for hospital admission. Furthermore, the economic burden of HF on the healthcare system is only predicted to increase with the increasing age average of the population, since the disease prevalence increase with increasing age and can reach over 10% for people over 70 years old [3]. Going forward, the healthcare system will face new challenges for improving the diagnosis of these diseases, the quality of life of the patients and the efficiency of treatments at an affordable cost. The process of HF diagnosis is difficult and challenging, since even if the pathophysiology of HF has been understood by the medical community in great extent the amount of potential clinical manifestation of an HF remains wide, with symptoms and causes being nonspecific to a single HF iteration [4]. In clinical practice, HF diagnosis is based on the examination of the patient and on the patient medical history and physical condition and is assisted by many different secondary tests. These tests range from the simple blood test to more complicated and expensive tests like magnetic resonance imaging, electrocardiogram and echocardiography, including more invasive and stressing

tests like cardiac catheterization [4]. Overall, the diagnosis process is long and requires a high amount of data, since usually HF are detected less frequently due to the nonspecific symptoms caused by the condition. In many cases, the HF condition is detected successfully only after the disease has progressed to an advanced stage [5]. Incorrected and undetected diagnosis lead to inadequate treatment for the disease, decreasing the quality of care provided and the quality of life of the patient. After the detection, even the therapy monitoring of the patient affected by HF is crucial for healthcare professionals and helps them tailoring the ongoing therapy to the patient needs, avoiding frequent re-hospitalization, increasing the quality of life and delaying disease progression to end stage HF.

In this framework inclusion of biomarker testing in diagnosis processes can provide great benefits, increasing the efficiency of HF diagnosis, making easier to monitor therapy and providing information about the mortality and risk for adverse effect of the affected patient. To be used as an effective tool easy, cheap and reliable solutions must be implemented. Point of care devices (POC) provide the best opportunities for the continuous and easy monitoring of these biomarkers, and the KardiaTool project aims to translate the already established laboratory concept of saliva biosensing to clinical practice for addressing the clinical needs in personalized HF diagnosis and patient monitoring at the point of care. Regarding HF diagnosis with biomarkers, clinical solutions exist using blood samples from the patient, but the use of blood as biological matrix implicates non-zero stress for the patient and exposes both the patient and the clinical assistant to risk of infections. Saliva has been proved to be one of the least invasive and most effective ways to identify pathophysiology conditions such as HF, being able to reflect the actual progression of the disease and provide diagnostic information. The main novelty brought by the KardiaTool platform is the clinical use of saliva to detect the insurgence of HF. While is common clinical practice to detect HF through the use of the biomarkers present in the blood [6], no available clinical study showed an efficient method to obtain the same accuracy through the use of saliva. The KardiaTool platform will be the first platform to show that is possible to obtain such results, and the main concepts of this novel platform are introduced in Figure 1 [1].

The KardiaTool is designed to fulfil ambitious goals: Its aim is to diagnose the HF by detecting the disease at an earlier stage, when it is easier and less expensive to treat effectively, reduce the time, cost and failure of misdiagnosis, monitor therapy of HF patients and stratify them into groups of high and low risk for HF event. The integration of the KardiaTool platform for diagnosis and therapy monitoring into the patient therapy process will provide the medical professionals with accurate,

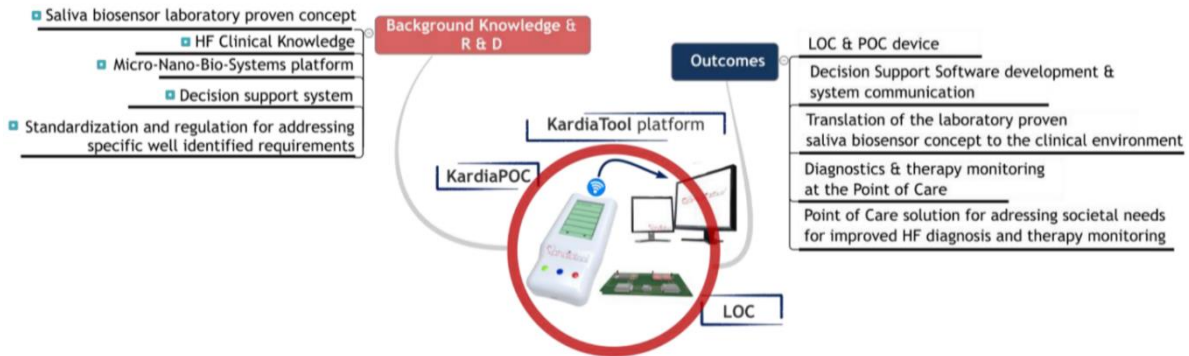


Figure 1. Main concepts of KardiaTool Project [1]

point of care results in less than an hour, improving the quality of life and quality of the treatment administered to the patients affected by HF.

To fulfil these objectives, in its final form the KardiaTool platform will include [1]:

- A portable and easy to use point-of-care device (KardiaPOC) with a disposable lab-on-chip (KardiaLOC) for the non-invasive, rapid and accurate qualitative and quantitative assessment of HF biomarkers from collected saliva samples. This device will integrate many different interfaces and a variety of sensors, actuators, bio-chemicals and functionalized magnetic nanoparticles.

- A decision support software (KardiaSoft), based on predictive modelling techniques, that analyses the POC data and other patient’s data directly added by the healthcare professionals and delivers information related to HF diagnosis and therapy monitoring to the technician.

The KardiaPOC will be an innovative point of care device compared to the commercially available ones and will insert itself in the gap existing in the accurate and on time diagnosis and therapy monitoring of HF: This is due to the incorporation of four saliva biomarkers and the simultaneous extraction of key information from them. The detection and quantification of these saliva biomarkers will improve the effectiveness and precision of the diagnosis, since specific high levels and fluctuations of these biomarkers is and indicator for the presence of HF [7]–[10]. Also, the use of saliva as testing sample instead of the more commonly used blood makes the device easier to

use and more acceptable for the patients and lowers the infection risk and the costs associated to the testing.

The challenge that the KardiaTool platform faces during the design, testing and fabrication process is triple:

- To translate a laboratory proven concept of a saliva biosensor into an MNBS platform for HF diagnostics and therapy monitoring at the point of care following the Good Laboratory Practice (GLP);
- To validate the MNBS platform through pre-clinical and clinical testing, following Good Clinical Practice (GCP);
- To industrialize the outcomes, following Good Manufacturing Practice (GMP) towards progress to marketisation

In this thesis the only aspects that will be treated are the ones related to the integration and characterization of some components of the KardiaTool platform. The following paragraph starts presenting an overview of the architecture of the platform.

1.1. KardiaTool general architecture

The KardiaTool platform architecture can be divided into 4 different layers; the first three layers being part of KardiaPOC platform and the last layer including the KardiaSoft software. The first layer includes the magnetic nanoparticles and the antibodies to functionalise them; the second layer includes the saliva samples, the chemical reagents that will be mixed with the saliva before the sensing, the microfluidic system and the immunosensor. These two layers are part of the LOC, a disposable device that will be changed for each testing session. The third layer includes the microcontroller, the memory storage, the battery and the interface necessary to communicate with the software that analyses the data via USB or Bluetooth. The components of this layer are integrated in the POC device, a non-disposable instrumentation that will be used for multiple testing session. The fourth and last layer includes the external decision support software, KardiaSoft. Figure 2 presents the different layers and the components of the KardiaTool platform:

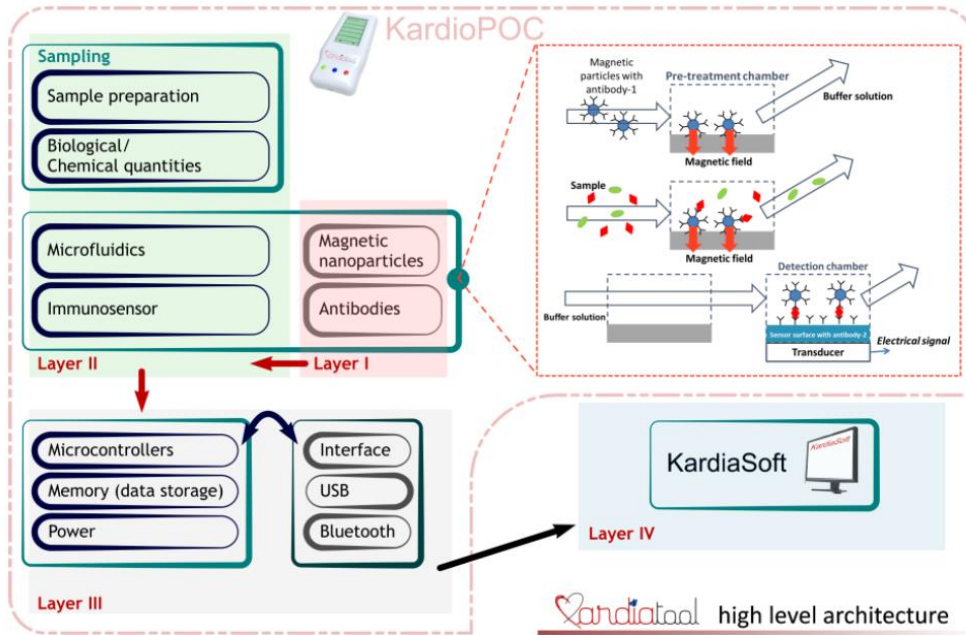


Figure 2. Kardiatool high level architecture

The integration of these different layers in a single device allows the healthcare figure to stay with the patient along the whole testing session, delivering a more personalized care. The organization of the different layers in a single device is explained through the following image, presenting the sequence of actions that the healthcare operator must perform to obtain clinical results from saliva samples.

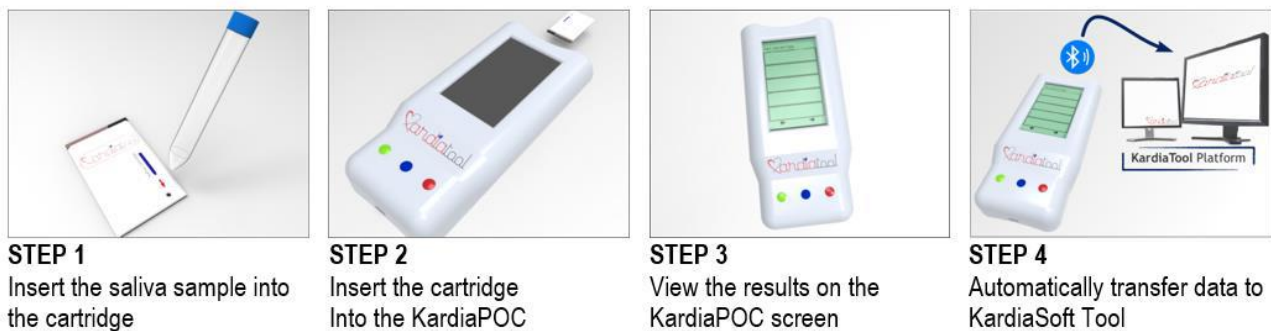


Figure 3. Working steps for Kardiatool functioning

Step 1: The healthcare figure collects the saliva from the patient, mix it with chemical reagents and MNPs and inject the final sample into the cartridge. The microfluidic behaviour of the sample inside the cartridge is managed by a pre-programmed sequence controlling a peristaltic pumping system. The sample undergoes different mixing and capture cycles in the coil chamber. After that, the MNP will be dispensed by the flow control in a second chamber and an electrical detection will be performed in a fully automatized fashion by a miniaturized FET immunosensor

Step 2: The healthcare figure loads the cartridge containing the immunosensor into the KardiaPOC instrumentation

Step 3: The results of the sensing performed by the FET immunosensor are displayed on the screen of the KardiaPOC. The different concentration of biomarkers is clearly visible.

Step 4: The biomarker results and other relevant clinical data are automatically transferred by the device to the external software KardiaSoft, where they are analysed to provide software-based healthcare related advice to assist the healthcare figure in the diagnosis and treatment of the patient

These steps are the general description of the work performed by the different components of the KardiaTool. In the following paragraph the complete workflow assay will be described, with attention to the description of the biomarker measurement procedure.

2. KardiaTool working assay description

In this section the description of the working process of the KardiaTool platform will be presented, from the collection of saliva samples to the analysis of data obtained from the KardiaLOC.

2.1. Biomarkers for HF detection

“A biomarker is a characteristic that can be objectively measured and evaluated as an indicator of normal biological processes, pathogenic processes or pharmacological responses to a therapeutic intervention “ [11]. The optimal biomarker should possess several different characteristics: It should be specific for a particular disease and able to differentiate between different physiological states; it should be safe and easy to measure; it should be rapid as to enable a fast and accurate diagnosis; should be cheap and able to give accurate results; and, lastly, should be consistent between different ethnic, age and gender groups. Moreover, the optimal biomarker should react swiftly in time, reflecting the changing in clinical status without a significative delay. Regarding the diagnosis of HF, the amount of candidate biomarkers that can be used to obtain a reliable diagnosis increased in time as the pathophysiology of the HF has been comprehended and defined, and they range from novel molecules to commonly used laboratory parameters.

The biomarkers used for the KardiaTool platform are the following four: NT-proBNP, TNF- α , Interleukin- 10, Cortisol. Here is presented a brief description of the four markers.

NT-ProBNP is a peptide that can be detected in the blood and in the saliva of both healthy and HF affected patient. The amount of this peptide is sensibly higher in heart failure patients and the concentration in plasma/serum of patients is currently used to clinically diagnose HF. The fact that this is an established biomarker for HF detection and the fact that it can be easily detected in saliva makes it a viable candidate for the KardiaTool platform [8].

TNF- α or Tumor Necrosis Factor Alpha is a chitochine involved in systemic inflammation and regulation of immune cells. This biomarker can be found in the saliva and in the blood of patients affected by HF, and is a biomarker clinically used for risk assessment in HF patient due to the elevated concentration that can be measured by analysing venous blood [12]. Different studies have underlined a profound impact of diabetes and HF on the amount of TNF- α in saliva as

compared to the amount shown in samples of saliva from healthy patients[7] and this made it an optimal choice for the KardiaTool.

Interleukin- 10 is an anti-inflammatory cytokine. Found in peripheral blood and in saliva, is usually used as biomarker for the detection of carcinoma, since the concentration of this cytokine is directly correlated. Medical studies shows that the concentration of this biomarker in saliva rises when the patient is affected by HF and this makes this biomarker a choice for KardiaTool [9].

Cortisol is a steroid hormone, usually used as a biomarker of psychological stress. The salivary cortisol concentration is an excellent indicator of the plasma free cortisol concentration, indicator that is directly related to the manifestation of HF phenomena. So, by measuring the concentration of cortisol in the saliva it is possible to verify the presence of an HF in the patient [13].

All these biomarkers were carefully chosen due to their biological characteristics, amount present in the saliva and clinical correlations with the presence of HF phenomena. The following paragraph provides a description of the method of detection for multiple biomarkers.

2.2. Biomarker measurement procedure

The main KardiaTool function is to produce a quantitative analysis of the biomarkers of interest present inside saliva samples. Since saliva is a complex biological matrix with a low concentration of the biomarkers of interest [14] the quantitative measure of the concentration of analytes increases considerably in complexity. To obtain a more precise measurement, the method employed consists in a self-calibration of the sample to be measured using a standard addition procedure. The standard addition method is used to determine the concentration of an analyte that is present inside a complex matrix, such as a biological secretion. The idea behind this method is to add a defined quantity of analyte to the sample and monitor the change in the feedback from the sensing instruments. The change in the sensor response between the sample and the sample with added analyte is assumed to be caused only by the change in analyte concentration. The usual procedure for standard addition consists in the splitting of the sample into even aliquots in separate volumetric containers of the same volume. A standard quantity containing the analyte is added in increasing quantities to the flasks and each flask is diluted to a volume with a selected diluent. If the analytical signal still changes proportionally to the concentration of the analyte even under the effect of the

matrix, it is possible to obtain a calibration curve using a simple linear regression. The analyte concentration before the addition of excess analyte can be extrapolated from the regression line [15].

In the KardiaTool device framework, 4 chemical solutions are prepared starting from the saliva samples and are stored in four disposable liquid reservoirs. The single biomarkers measurement is based on two steps: The first step consisting in an initial mixing, incubation and pre-concentration and the second step consisting in the detection of the quantity of analytes. These two steps require two separated fluidic chambers to be carried on. MNPs are used as the vehicle for the pre-concentration and the controlled transport between the two chambers. The structure of the fluidic system is schematized in Figure 4.

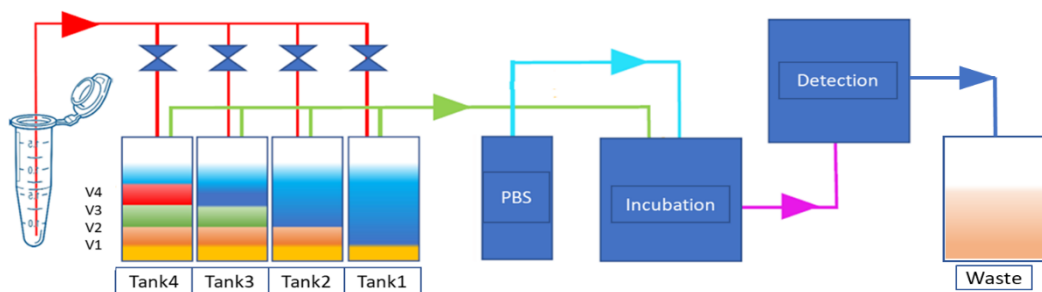


Figure 4. Schematization of KardiaTool fluidic system

Here are represented the 2 chambers for incubation and detection, placed one after the other and connected to the waste tank. The incubation chamber contains magnetic coils capable to generate a magnetic field that will be switched on and switched off depending on necessity. The detection chamber contains the functionalized biosensor. Four tanks containing different concentration of the biomarker of interest and a tank containing the buffer solution are placed before the two chambers. Each tank contains the same concentration of saliva and different concentrations of the biomarkers to measure. The four solutions are prepared in the four tanks and their composition is the following:

V1: Consists of saliva sample. The same amount of saliva is added to each tank.

V2: Consists in the same volume of a standard solution that is added to the tanks 2,3,4. This standard solution contains the same concentration [C1] of the four biomarkers.

V3: Consists in the same volume of a standard solution that is added to the tanks 3 and 4. This standard solution contains the same concentration [C2] of the four biomarkers.

V4: Consists in the same volume of a standard solution that is added to the tank 4. This standard solution contains the same concentration [C3] of the four biomarkers.

The first tank contains the buffer and the saliva sample V1; the second tank contains the buffer, V1 and V2; the third tank contains the buffer, V1, V2 and V3 and the last tank, the fourth, contains the buffer, V1, V2, V3 and V4. To all the four tanks is added a specific quantity of magnetic nanoparticles and a given volume of buffer solution, 1-2 ml.

The measurement procedure for a single biomarker and for multiple biomarkers will be now explained.

2.3. Pre-measurement procedure

The measurement procedure starts with adding the same quantity of saliva sample to the four tanks. After that the magnetic nanoparticles are added to each tank. The tanks are shaken, and some time is left to pass for a defined incubation time. After the incubation time, the biomarkers are bound to the functionalized magnetic nanoparticles present in the sample and the measurement procedure can begin.

2.4. Single measurement and complete measurement procedure

The procedure for the detection from one tank is summarized in the following points:

- 1) The tank is inserted in the device and the sample solution flows into the incubation chamber.
- 2) In the incubation chamber the magnetic coils are switched on for a defined capture time, generating a magnetic field. The magnetic particles are fixed by the coils present in the magnetic chamber for a defined incubation time, as shown in Figure 5.

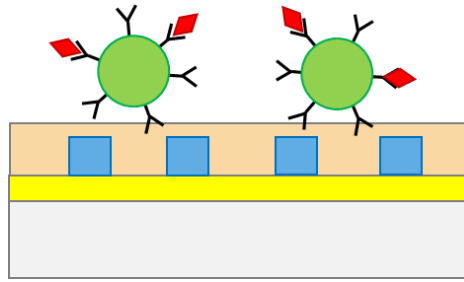


Figure 5. Magnetic particles with captured biomarkers fixed to the coils

- 3) The incubation chamber is then washed by an appropriate buffer. This passage eliminates the non-bound interfering substances and reduce the effect of the variability of the saliva matrix. The buffer liquid flows out to the waste reservoir.
- 4) Next, the coils in the incubation chamber are switched off as is the magnetic field. The magnetic nanoparticles are released from the incubation chamber and free to flow.
- 5) A carrier buffer is released in the channel and the magnetic particles are moved into the detection chamber integrating a biosensor.
- 6) In the detection chamber the magnetic nanoparticles are detected by a functionalized biosensor, as shown in Figure 6. The biosensor surface is functionalized with an antibody that is saturated with the biomarker molecules. The magnetic nanoparticles will bind to the surface of the biosensor only if they have one or more antibody that is not saturated by a biomarker.

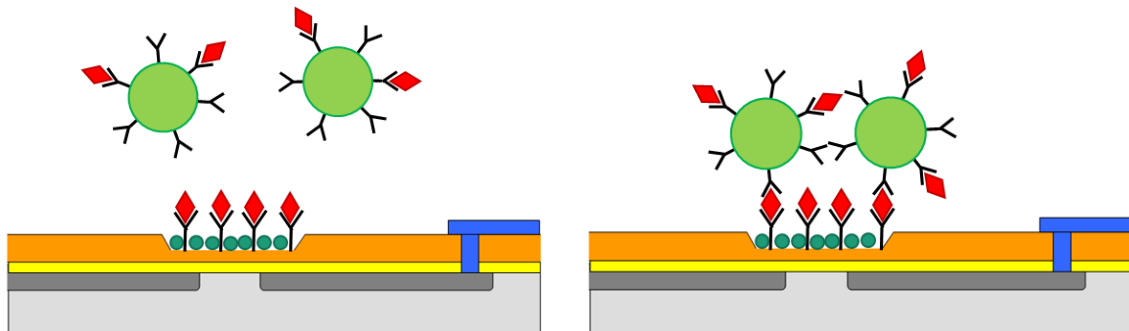


Figure 6. Bonding of the magnetic particles into the functionalized surface of the biosensor

In this situation, a high concentration of biomarkers will result in magnetic particles saturated by biomarkers and these saturated magnetic nanoparticles will not bond to the surface of the ISFET and in result produce no signal. A low concentration of biomarkers will result in magnetic particles with many free antibodies, which will bond to the biosensor surface producing a large signal.

- 7) After a certain required diffusion time and an antigen-antibody reaction time, the particles that were not bonded are removed by a carrier buffer that flows into the detection chamber to the liquid waste tank.
- 8) The last step consists in flushing the detection chamber with the buffer and following take the measurement from the biosensor is obtained.

This procedure, that is used for the detection of a single biomarker, can be adapted for the measurement of four different biomarkers using the standard addition method. To perform a complete measurement for all four biomarkers, the procedure described in the previous paragraph is repeated four times measuring the samples consecutively from tank 4, tank 3, tank 2 and tank 1. Since the antigen-antibody bonds are permanent, the biosensor surface can't be regenerated after each measurement. Due to the competition measurement methodology, described in step 7 above, for the higher concentration solution (tank 4) there will be a low binding of the nanoparticles to the immuno-ISFET surface. Therefore, most of the surface will be free for the next measurement. In this way, the four measurements can be performed, even though the surface coverage by the nanoparticles will increase from the first measurement (tank 4) to the fourth one (tank 1).

3. KardiaTool LOC/POC design and specification

The following paragraph describes the design specification and the working principles of the LOC. As described in the previous paragraphs, the KardiaTool platform will be composed by different parts, those being the external software, the Lab-On-Chip part and the Point-Of-Care part. From the hardware point of view, the difference between the POC and the LOC consists in the fact that the LOC is a disposable device and the POC is a permanent system that will be re-used multiple time. The complete structure of the POC and the LOC is defined and presented in Figure 7.

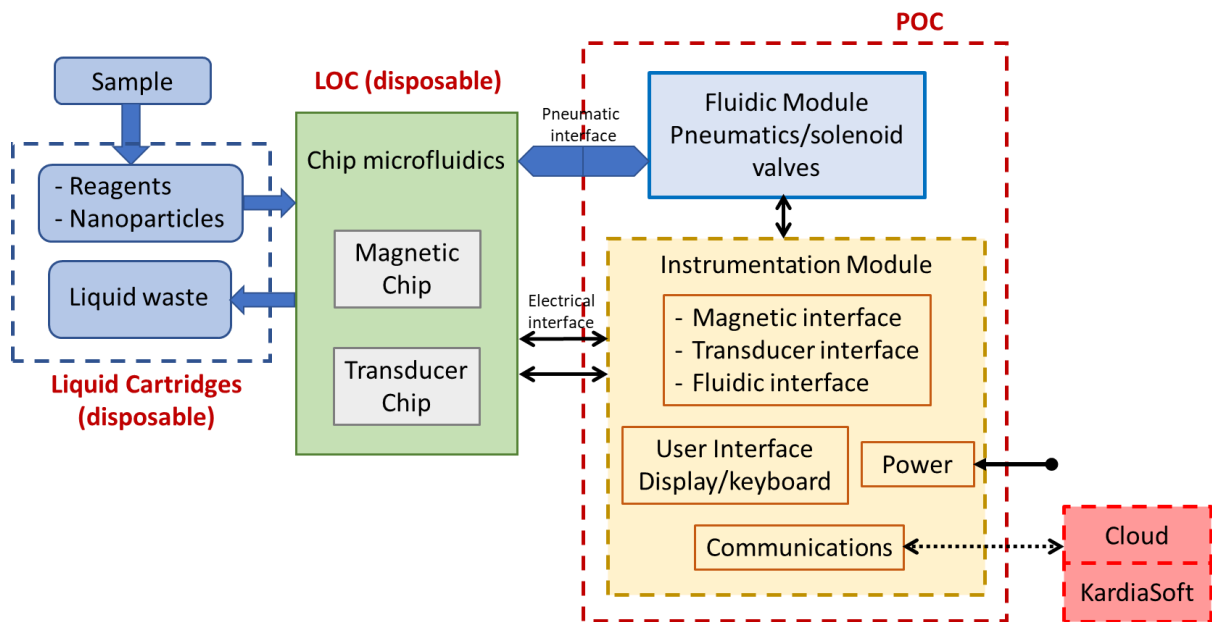


Figure 7. LOC and POC diagram description

The two components are well defined and contain several different modules interconnected between them. The LOC contains the microfluidic chip, the magnetic chip and the transducer chip than are bonded into the microfluidic chip. The LOC interacts with the liquid sample through a fluidic interface (small tanks filled with liquid are inserted into the microfluidic chip) and with the POC through a pneumatic and electrical interface (a system of electrical connections and pneumatic connection between the pneumatic valves and an external pump). The POC is a more complex device, containing instrumentation modules to control and monitor the components and the LOC. A more schematic view of the LOC is presented in Figure 8 :

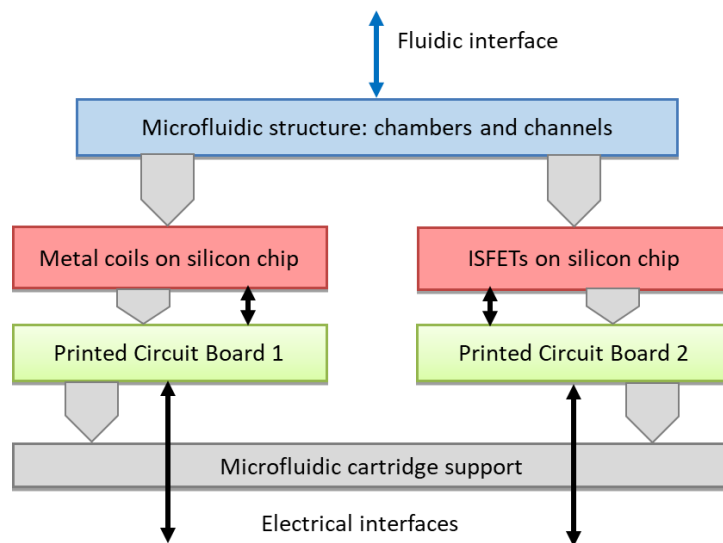


Figure 8. LOC schematic

As said before, the LOC includes the microfluidic cartridge, the biosensing chip and the magnetic chip. All these components are disposable and are used for a single testing session. The LOC is built to accommodate for disposable liquid cartridges that contain both the sample mixed with reagents and MNPs and the liquid wastes. Pneumatic connections are inserted in the microfluidic cartridge and let the LOC control the pumping and valving system, and the information obtained by the biosensor are passed to the POC through electric connections. Figure 9 presents a visualization of the components of the LOC physically assembled:

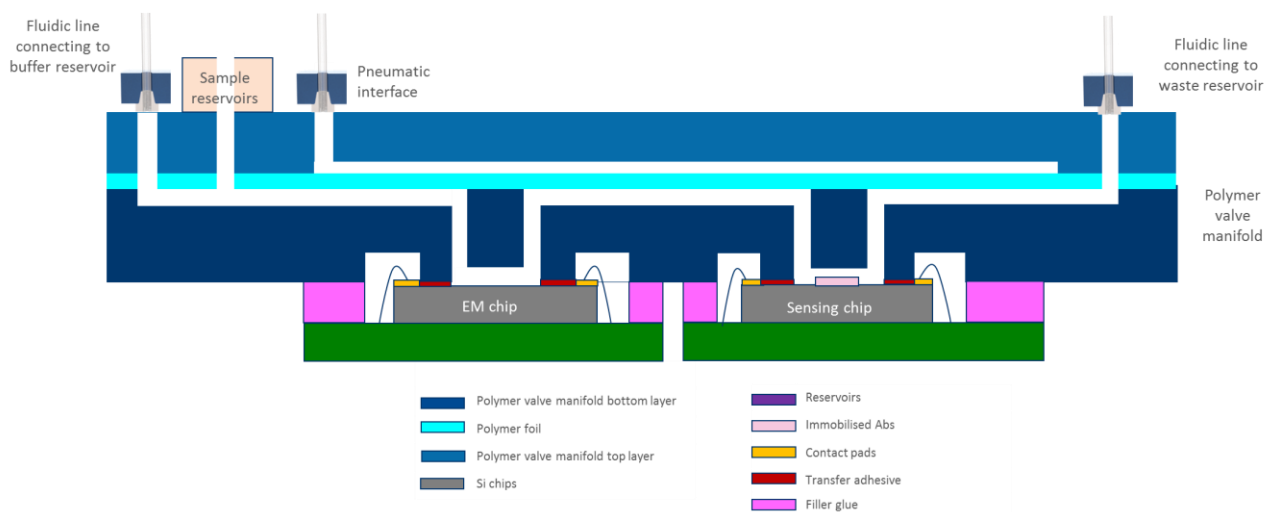


Figure 9. Schematic representation of the microfluidic system integrated in the disposable LOC

The whole LOC is installed on a PCB board that is used as electrical interface between the LOC and the POC. Two silicon chips are installed on the PCB: An ISFET biosensor and an electromagnetic chip, both having a functionalized surface. Both chips have bonding pads and electric connections inserted in the PCB. Both chips are bonded to the microfluidic chip through the dispensing of an adhesive glue, and a filler glue is present between the microfluidic chip and the PCB to stabilize the system. The polymeric chip is composed by three different layers, one polymer valve manifold bottom layer, one polymer valve manifold top layer and a polymeric foil between them. These three layers are assembled to form the microchannels and the fluidic valves used to control the flow of the liquid inside the cartridge. On top of this polymeric cartridge are the pneumatic connection, connecting the pneumatic elements in the cartridge with the external actuator, the sample reservoir containing the saliva samples and the fluidic lines connecting to the buffer reservoir and to the waste reservoir.

In the following paragraphs the different components of the LOC will be described in detail, with attention to the existing solutions for LOC technology and the design choices behind the integration of the different layers.

4. KardiaTool components description

In this chapter each component of the KardiaTool device will be describe, with references to the state-of-the-art technology behind each one of them. The first paragraph will describe the microfluidic cartridge, highlighting its components like the microfluidic valves and the integrated pumping system; the second paragraph will describe the magnetic nanoparticles; the third paragraph will describe the electromagnetic planar coils that are integrated in the microfluidic chip; the last paragraph will describe the biosensor that will be used for the detection of the MNPs, an ISFET.

4.1. Microfluidic cartridge

The scope of this part of the work revolves around the presentation of the design of the polymeric cartridge used in the KardiaTool device. The first prototypes fabricated were disposable thermoplastic cartridges, made in polystyrene. These prototypes incorporated all the features useful for the project and the integration in the KardiaLOC, such as an interface for reservoir, waste, buffer and pneumatic actuation on one side of the chip as well as two different chambers on the other side, one for the accommodation of the ISFET sensing chip and one for the accommodation of the electromagnetic coils. These elements are interconnected by a fluidic network, passing through the whole chip and connecting the samples with the waste through the two chambers. The cartridge also integrates many valves and a micro-pump and uses a pneumatic network for flow control in order to enable performing the various steps of the assay of the Point-of-Care device. A prototype of the polystyrene cartridge fabricated during the project is show in Figure 10.

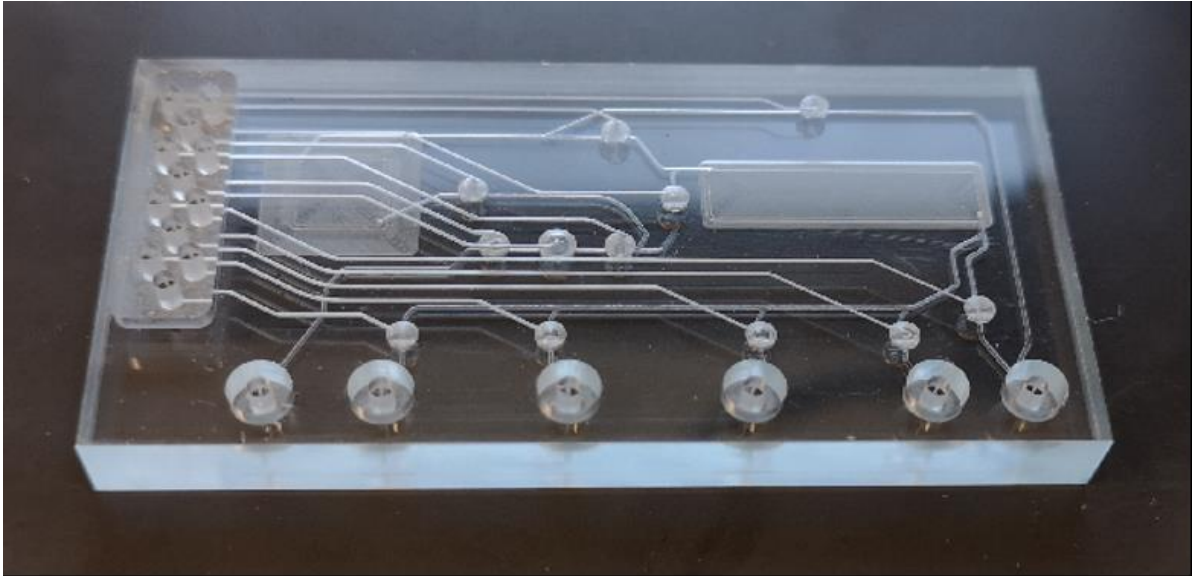


Figure 10. A prototype of the microfluidic cartridge

The design of these microfluidic cartridges revolved around the fulfilling of some required specifications:

- The material used for the fabrication needed to be thermoplastic to provide a cheap and disposable system
- The fabrication needed to rely on cost effective manufacturing equipment and processes that can be scaled to higher level manufacturing for industrial production
- The design had to provide a functional microfluidic system enabling the KardiaTool assay, able to integrate flow control and the reservoir
- The design had to enable the use of an external controller able to control the flow of the liquid in the device

In addition to complying with these specifications, the LOC cartridge must perform a certain number of steps in a given order. This sequence defines the fluidic network required and the number of elements to be incorporated. Figure 11 gives a brief description of the theoretical microfluidic network necessary for the complete function of the chip and the steps the cartridge must perform during a normal working assay. The main components of the polymeric cartridge are presented in this theoretical schematic, such as the microvalves, the two inner chambers and the different tanks for the samples and the buffer. The fluidic network is designed in order to perform the steps necessary for the assay in a simple way.

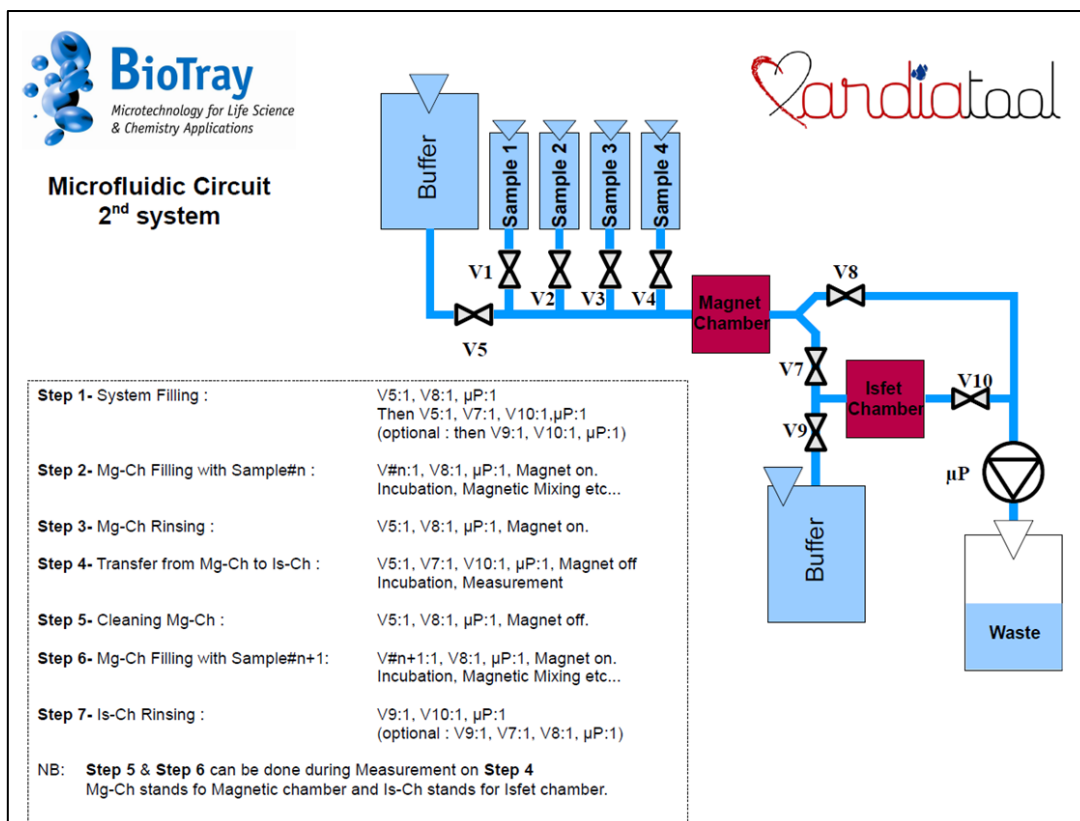


Figure 11. Schematic of the fluidic network and description of the steps needed to perform the KardiaTool assay in the LOC. The components of the microfluidic system are highlighted, such as the valves and the chip chambers

From this theoretical schematic the design was finalized to obtain the cartridge introduced in Figure 10. The polymeric cartridge has a footprint of 30*60 mm and a total thickness of 6.1 mm. The fabrication of the cartridge was performed by structuring 5 layers of polystyrene, 4 plates and a flexible membrane. Three main layers compose the cartridge, one pneumatic layer that allocates the pneumatic lines connecting the external pumping system with the microvalve, one thermoplastic middle membrane layer that constitutes the moving membrane for all the different microfluidic valves and one fluidic layer allocating the channels in which the liquid flows. These different layers were then stacked and bonded using a solvent-assisted thermal bonding method. The different layers are presented in detail in Figure 12.

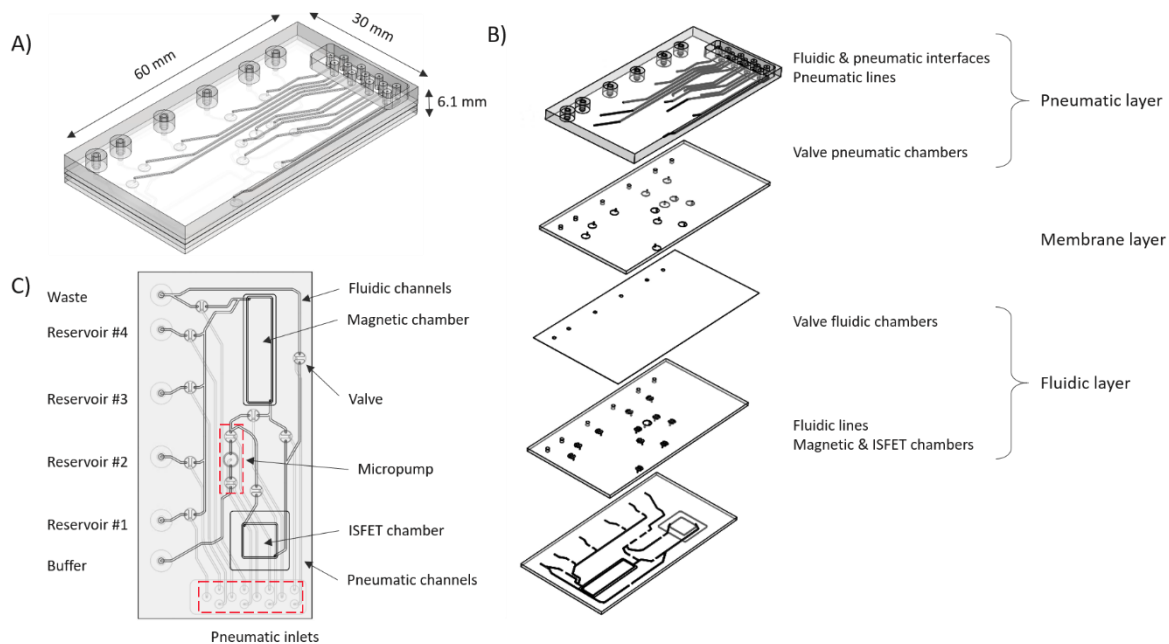


Figure 12. Microfluidic cartridge prototype design: A) 3D isometric view of the cartridge prototype. B) 3D exploded view showing the 5 layers composing the cartridge. C) View from the chamber side and description of the different elements.

The pneumatic and fluidic layers are further divided of 2 sub-layers. For the pneumatic layer, the 1st sub-layer (3 mm thick) incorporates on its upper side the interfacing for the sample reservoirs, and the fluidic and pneumatic lines and, on its bottom side, the pneumatic lines. The 2nd sub-layer (1 mm thick) hosts the pneumatic chamber of the different valves to which connects the pneumatic lines above. Regarding the fluidic layer, its top sub-layer (1 mm thick) gathers the fluidic chambers of the valves. Its bottom sub-layer (1 mm thick) possesses on its upper surface the fluidic lines connecting the inlets, valves and the 2 main chambers that are present on its other surface. The fluidic layer layout, better visible in Figure 12.C, accommodates to the one from. Through holes are made in the four upper layers to allow access from the fluidic inlets to the fluidic lines on the last layer. The fluidic and pneumatic inlets exhibit a pillar shape in order to later attach flexible tubing for fluidic tests, avoiding the need to develop a specific holder for interconnections. In the final version, these inlets will become simple holes since ferrules will be used to interface rigid tubing with the cartridge. The fluidic channels are 320 μm wide and 150 μm deep. Their cross-section dimensions have been defined using a best estimate according to expected flow rates to be used inside the cartridge. Further experiments on Micronit test bench will conclude if they need to be modified. The valves exhibit the same depth as the fluidic lines and a diameter of 2 mm. Only the centre valve of the pump has a larger diameter of 2.5 mm. The magnetic and sensing chambers

footprint have been dimensioned according to the latest design to date provided by the partners of Micronit responsible for the fabrication of both silicon chips. Their position allows for the chip and the PCBs having some spacing between them. The height of the magnetic chamber has been set to 100 μm to maximize the capture of MNPs based on simulation provided by the partner. To offer a similar chamber volume, the sensing chamber is 300 μm high. The chamber walls are 250 μm wide and with a height comparable to their chamber. The microfluidic chip hosts 13 pneumatic valves as shown in detail in Figure 13, and three of these valves constitute the pneumatic peristaltic pump and are actuated in rapid succession during the whole actuation period. Regarding the peristaltic pump, the first and the third valve are equal in dimensions while the second valve is bigger, having a diameter of 2.7 mm compared to the standard diameter of 2 mm. This intermediate valve is the one in which the fluid accumulates during every pumping cycle. All the other valves are numerated and placed carefully to fulfill the design specification previously highlighted. The valves are operated to actuate the different steps in the sensing process and during all these steps the pumping system is always active. The valves from 1 to 4 are used to control the flow of the liquid from the respective sample tanks. V7, V8 and V9 are activated at the same time to fill the ISFET chamber during the sensing step. The buffer valve V5 is positioned upstream to limit the cross contamination between samples when filling the magnetic chamber. The second buffer line and the valve V9 directly connected to the ISFET chamber are added to being able to clean the ISFET chamber without flowing the liquid through the magnetic chamber. It is also possible, in case a more compact design is needed, to have a channel from valve V9 to the first buffer reservoir. The valve V10 is added to isolate the ISFET chamber from the waste container, and the micropump is positioned downstream of the whole system. V6 is not present in the numeration of the valves. The pumping system is always active when the system is active and generates a difference of pressure between the buffer/samples chamber and the waste reservoir. Once the cartridge was fabricated several functional tests were performed to validate and characterize the flow control that was achieved. Reservoir prototypes were developed and used for more realistic testing. The integrated valves

proved to allow or block the flow while pumps deliver a stable flow rate from 90 $\mu\text{l}/\text{min}$ up to 250 $\mu\text{l}/\text{min}$.

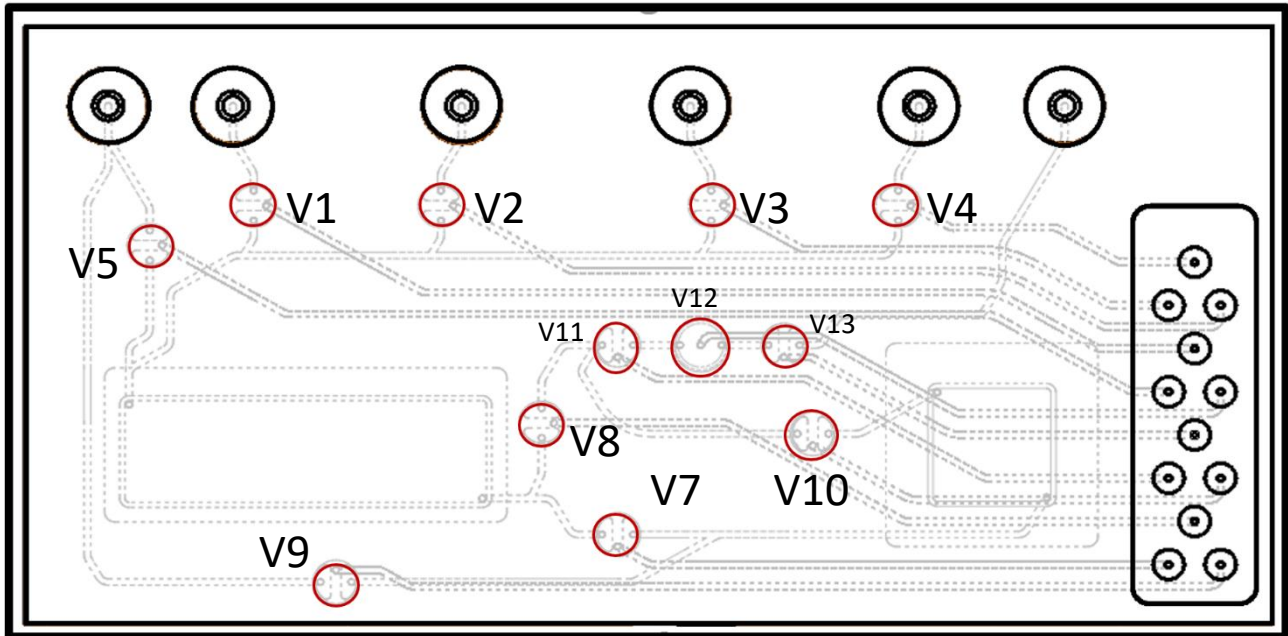


Figure 13. Layout and numbering of the microfluidic valves in the chip

4.2. Fabrication of the microfluidic cartridge

The design shown in Figure 10 has been fabricated in polystyrene due to the particular properties of the material and the requirement from the process. The process steps used for fabrication are described in general in Figure 14. During a first step, a micro-milling machine structures 4 PS plates and a cutter plotter structures the membrane. Then the various layers go through a surface treatment step where they are exposed to solvent vapours. Once treated the 5 layers are stacked and aligned together and then bonded using a thermal bonding machine that applies heat and a high pressure. Thanks to the surface treatment, minimal deformation of the structures is guaranteed since bonding is performed at a lower temperature than the glass transition temperature of the polymer (i.e. temperature at which the polymer goes from a hard state to a viscous one). Eventually, the bonded stack is milled to provide individual chips.

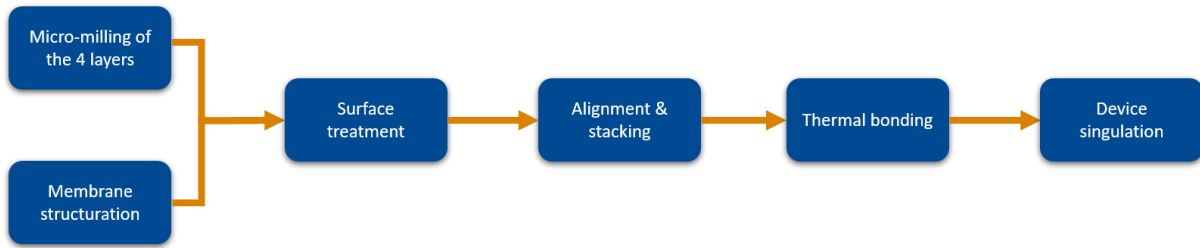


Figure 14. Process flow for the fabrication of the thermoplastic disposable cartridge prototypes.

The size of the plates allows fabricating up to 8 chips per fabrication run ensuring a cost-effective fabrication. Figure 15 shows a front view the result of a cartridge fabrication obtained following the process described above.

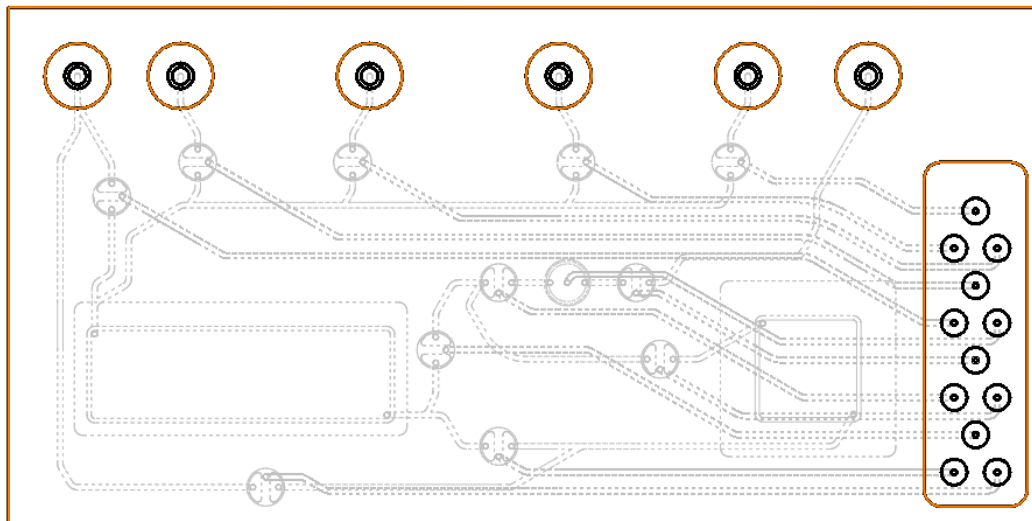


Figure 15. front view of the polymeric cartridge

4.3. Reservoir prototypes

In this paragraph are presented some insight on the prototype tanks that were used during the different experiment. A rapid prototyping has been made to fabricate reservoirs for the functional tests. These reservoirs are made using 0.5 mL Eppendorf® tubes pierced at their bottom. A flexible PTFE tubing is cut to a few millimetres in length and is slightly inserted inside the bottom opening of the reservoir. The outer diameter of the tube is chosen such that the tubing is inserted with a slight resistance. To mount the reservoir on the cartridge, the tubing is fitted onto an inlet pillar (Figure 16.A). As shown in Figure 16.B, this strategy provides a leak-free reservoir solution.

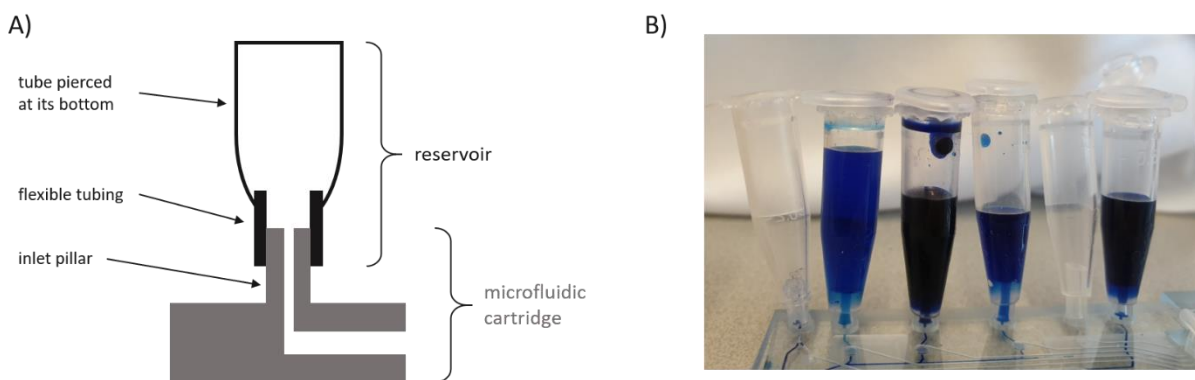


Figure 16. Reservoir prototyping. A) Schematic of the cross section of the reservoir mounted on the microfluidic cartridge. B) Picture of the reservoirs assembled on the fluidic cartridge and filled with a blue-stained liquid.

This configuration was considered only for the testing set-up, and investigations are currently being run in order to define the reservoirs, and their features, to be integrated better in the KardiaLOC.

4.4. Microfluidic Valves working principles and functionality

Microvalves and micropumps are the essential element of many different microfluidic systems for various applications, as they allow the users to control the flow of a fluid in a microchannel by varying a macroscopic parameter like pneumatic pressure [16]. A careful design of microfluidic valve is essential to control the routing and the separation of fluids within a device, especially in designs with high complexity. Micropumps are pumping systems integrated in the microfluidic device and are responsible for the generation of a fluid flow within the device. Microvalves can be active, requiring an external actuation to work, or passive, requiring no external actuation. Active valve can be further divided into categories depending on the actuation method as they can be actuated mechanically, pneumatically, electrokinetically, by phase change or by introduction of external forces [16]. For applications that requires multi step operation on a single device with high throughput and especially microfluidic biomedical applications, elastomeric pneumatic microvalves have shown to be a strong and reliable choice [17]. Many examples in literature show successful application of pneumatic valves in Lab on chip systems in applications such as cell sorting [18], DNA sequencing [19] and protein-antibody interaction screening. This kind of valve, introduced by Stephen Quake [20] use the deflection of a polymeric membrane (usually PDMS) to control the flow of the liquid in the channel. The pressure is applied to the membrane through a dedicated line usually called the control line. They are one of the most used kind of valve due to the fact that can be easily integrated in microfluidic systems using standard lithography processes [21]. The most common classification of pneumatic microvalves consists in two main categories: Normally Open (NO) valves and Normally Closed (NC) valves. Normally open pneumatic valves are designed to block the flow of the fluid only when a positive pneumatic pressure is applied, while normally closed valves require a negative pressure applied to let the fluid flow in the channel [22]. For the design of the microfluidic chip present in the LOC the design team decided to implement NC valves in the microfluidic chip, actuated by an external pneumatic pump.

The design of the valve used for the polymeric chip is show in Figure 17.a). The valve is constituted by 2 different polymeric layers, one fluidic upper layer in which the liquid flows through a channel and a pneumatic layer, connected to the external actuating pump. The middle layer is an elastomeric layer that is deflected by the external applied pressure to open the microfluidic channel. Another prospective of the monolithic valve can be seen in Figure 17.b). When vacuum is applied to the

pneumatic channel, the thermoplastic membrane is sucked in the displacement chamber and the liquid is free to flow through the fluidic channel. The valve is normally closed, but in the normal working process a positive pressure is applied to the membrane to keep it shut and to balance the pressure of the liquid. As described in the previous paragraph, there are 13 microfluidic valves in the polymeric chip, and three of those valves placed in succession constitute the integrated microfluidic pumping system.

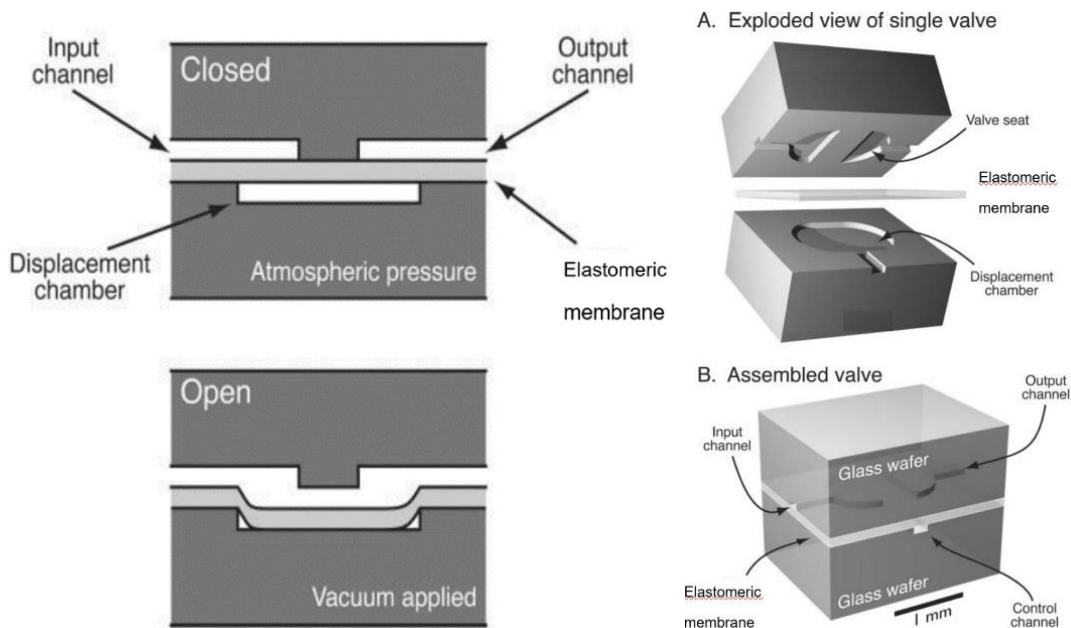


Figure 17. A) Microfluidic valve component design cross section [22]. B) exploded and assembled view of a valve [22]

4.5. Integrated microfluidic pump

In the microfluidic cartridge the pumping system is composed by three valves placed one after the other, V11, V12 and V13 as labeled in Figure 13. Figure 18 presents a detail of the three valves taken from a functioning microfluidic chip. The two external valves have dimension equal to the other valves present inside the polymeric cartridge, while the middle one functioning as the main pneumatic chamber is slightly bigger, having a 2.7 mm diameter compared to the standard 2 mm.

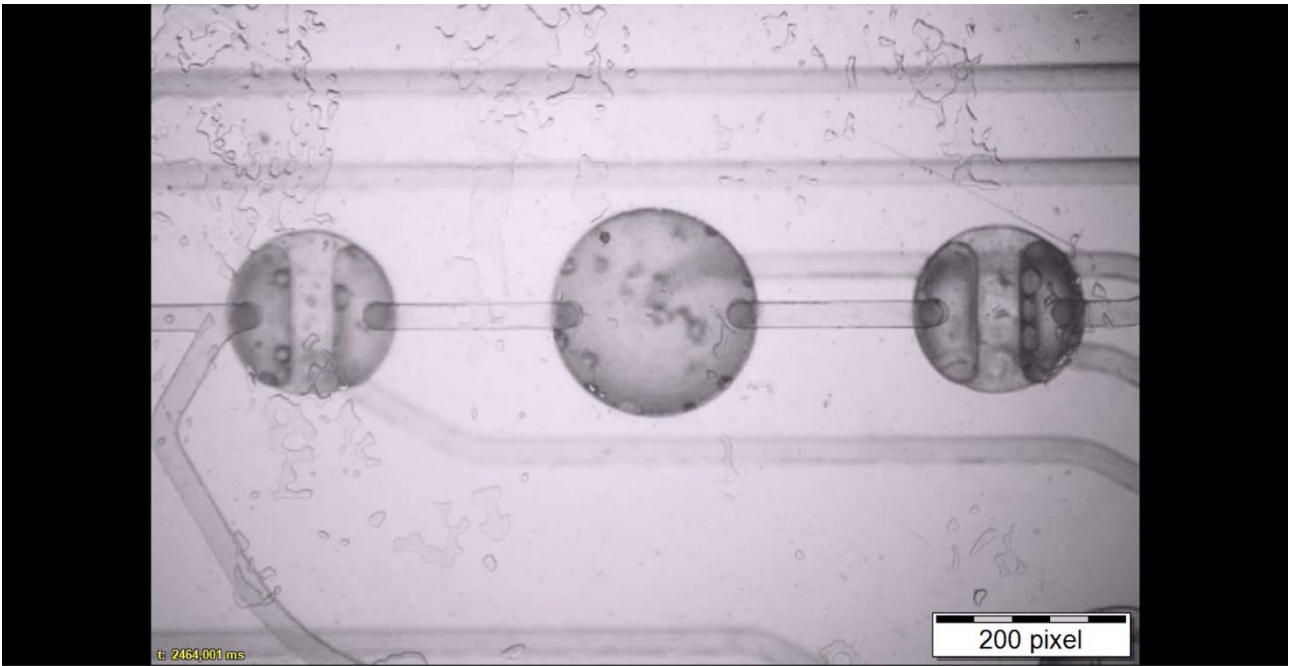


Figure 18. Image of V11, V12 and V13, forming the internal peristaltic pump

The three valves are actuated in succession by the external pumping system following a specific cycle that is repeated for the duration of the working period. The working routine of this peristaltic pump is presented in Figure 19:

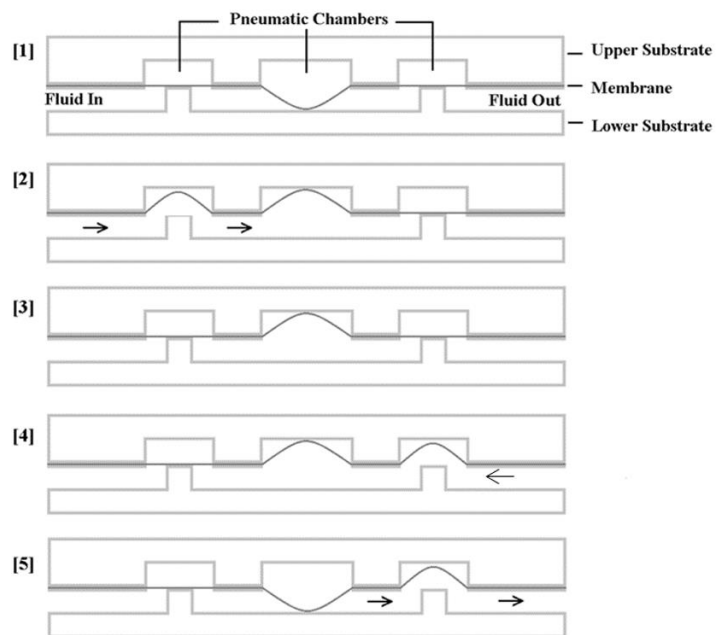


Figure 19. Working routine of the peristaltic pump

The system starts in idle state, with the three valves closed and with the membrane of the middle valve filling the lower volume of the chamber. The first step in the pumping sequence consists in opening the first and the middle valve. This generates a negative pressure due to the change in volume in the middle chamber, causing the liquid to move to fill the new accessible volume. The first valve is then closed to prevent the backflow of the liquid during the following steps. The last valve is opened and consequently the middle valve is closed, pushing the liquid accumulated inside the chamber in the microfluidic channel. This process takes the name of “pneumatic cycle” and in the KardiaTool platform can be repeated for a pre-determined number of times, from a minimum rate of 50 cycles/minute to a maximum rate of 150 cycles/minute. This Peristaltic pump was tested and characterized during the testing sessions, and the results of those characterization testes will be presented in the following chapter.

4.6. Functionalized magnetic nanoparticle

Magnetic nanoparticles (MNPs) are a class of engineered particulate material of diameter <100 nm that can be manipulated under the influence of an external magnetic field. MNPs are normally composed of magnetic elements like iron, nickel, cobalt, magnetite, maghemite, cobalt ferrite [23]. Generally, in the medical field they provide the ability to be directed and concentrated within a target tissue by mean of an external field and to be removed from the location after the therapy is completed. Moreover, particles in the range of 10-30 nanometres diameter can display superparamagnetic properties, not keeping the magnetization after the action of the magnetic field and so reducing the risk of particle aggregation [24]. In the absence of an electromagnetic field, the net magnetic moment of an MNP is zero at high enough temperature and when a magnetic field is applied to the MNP, a magnetic dipole is induced and this produces a net alignment of magnetic moments. After the external magnetic field is removed, the MNPs randomly orient and return to their native non-magnetic state. The magnetic properties are based on the magnetic susceptibility of the material, being the ratio between the induced magnetization and the applied magnetic field. MNPs from ferrimagnetic and ferromagnetic materials have ordered magnetic states and each MNP become a single magnetic domain, maintaining a large magnetic moment. These properties change at high temperature, but this influence is neglected for biomedical applications. In sensing application and also in KardiaTool, MNPs are integrated in the transducer materials, and/or a dispersion of MNPs in the sample is followed by their attraction by an external magnetic field onto the active detection surface of the biosensor. MNPs have a large surface area, and their surface properties can be tailored during the production process for a whole diversity of application, such as biosensors or other sensing systems. The methods of preparation of MNPs are various, some being precipitation from solution, high temperature decomposition of organic precursors, microemulsion, aerosol [25]. The least efficient methods for production of MNPs are the physical methods (e-beam lithography and gas phase deposition), being ineffective in the control of the particle size efficiently at nanometric scale while the chemical methods ensure a better yield, good reproducibility and ensure particle stability.

To prevent irreversible agglomeration and to enable dissociation, MNPs need to be stabilized. Such stabilization is commonly done by surface coating using appropriate polymers/surfactants, such as dextran, and poly (ethylene glycol)], or building lipid-like coatings around the magnetic core.

For KardiaTool, the particles used are provided by our partner, and are amino-dextran MNPs with average diameter of around 50 nm. The particles are MNPs with diameter of 200 nm. They are functionalized by our partners and are mixed with the samples of saliva for the standard working assay. The MNPs will be localized onto the biosensor through an antibody-antigen reaction between the surfaces of the MNPs and the biosensor that are properly functionalized. A more in-depth analysis of the utilized MNPs is presented in the following chapters, where the results of different testing session is presented. The particles were deemed compatible with the normal working routine of the microfluidic chip and no sign of clogging or obstruction of channels is noted during the process.

4.7. ISFET immunosensors

Immunosensors are affinity ligand-based biosensor solid-state devices in which the immunochemical reaction is coupled to a transducer [26]. At the base of all immunosensing technology there is the specificity of the recognition of antigens by antibodies to form a stable and strong complex. Generally, immunosensors can be divided into two major groups: Labeled immunosensor and label-free immunosensor. Labeled immunosensors require a secondary molecule or amplification step for the detection process, while label-free immunosensors directly detect the molecule of interest. A labeled detection method captures the analyte of interest using primary antibodies and detect the bound analyte using fluorescent molecules attached to the secondary antibody. A label-free sensor, on the contrary, can directly sense the binding between the biomarker and the antibody [27]. Label free detection is considered a direct detection mode and allows to monitor the binding of biomarkers in real time. A Labeled detection, on the contrary, is more reliable than a label-free detection and has a higher sensitivity, but needs larger volume of samples, long incubation period, complex auxiliary devices and highly trained staff and this impact considerably on the amount of resources and money used for these processes. Label free immunosensors allow for the direct monitoring of immunoreactions by measuring the biochemical changes due to the interaction between the antigen-antibody. In the KardiaTool LOC, the sensor used to assess the presence of the biomarkers is an Ion-Sensitive Field Effect Transistor (ISFET), a label-free immunosensor. The ISFET was preferred to an labeled solution in order to reduce the impact of the resources that are necessary during the detection process, especially the amount of sample employed and the incubation period. The ISFET is a type of potentiometric device that operates in a way like the way the MOSFET works.

Principles of FET biosensors

A FET generally consists of three distinct terminals: The source, the drain and the gate. The voltage applied to these three terminals regulates the flow of the current between the source and the drain. This current control mechanism is determined by the electric field that is generated by the voltage applied to the gate. The current in the device is conducted by only one type of carrier depending on the Type of FET, electrons for n-channels FET and holes for p-channels FET. When a positive voltage is applied to the gate of an n-FET, the free holes are pushed away from the region of space under the gate and a depleted region is generated, populated by the bound negative charges. The voltage

also attracts free mobile negative charges from the substrate to the depleted region. When the voltage applied is above a certain threshold a thin n-channel is created, connecting electrically the source and the drain region. This channel is formed by inverting the substrate surface polarity, from p-type to n-type, creating an inversion layer. After the creation of this channel, when a voltage is applied between the drain and the source a current is generated through the n-channel via the mobile electrons. In case of a p-type semiconductor, applying a negative voltage leads to a creation of a p-channel below the gate and increase the conductance, while the application of a negative voltage accumulates the carriers and increases the conductance (opposite to the effect present in the n-FET). The gate voltage generates an electric field that develops in verticality and that controls the amount of charge in the channels and the conductivity. The gate voltage that is applied to accumulate a sufficient number of charges and generate a conducting channel is the threshold voltage, V_{TH} . V_{TH} is positive for a p-channel FET and negative for an n-channel FET.

The FET can be configured as biosensor by modifying the gate to include molecular receptors or ion-selective membranes for the analyte that needs to be measured [28]. When the biomolecule, that is charged, binds to the terminal results in an accumulation or depletion of charges caused by the change of total charge on the gate terminal. In short terms, the electric field generated from the binding of a charged biomarker to the gate is analogue to applying a voltage to the gate, and measuring the current is possible to determine the number of biomarkers bonded to the biosensor.

In the ISFET, Ion sensing field effect transistors, the gate is an ion-selective membrane coupled with a reference electrode. The amount of current flowing is the amount of the current flow will be not only determined by the charges of biomolecules interacting on the gate dielectric, but also sensitive to pH, different ions, products of enzyme reactions, etc[28]. With such FETs, is possible to detect biomolecular interactions in a label-free manner through a change in electrical properties, like the conductance. Figure 20 presents a basic representation of the ISFET, with attention to all the different components. ISFETs are used in a variety of application in the biosensing field, like immunological sensing, living cell response sensing and DNA sensing [27]. This is due to the particular merits of the ISFETs, that are suitable for use in miniaturized measurement systems and portable devices, with the final integration that is characterized by small size and low weight.

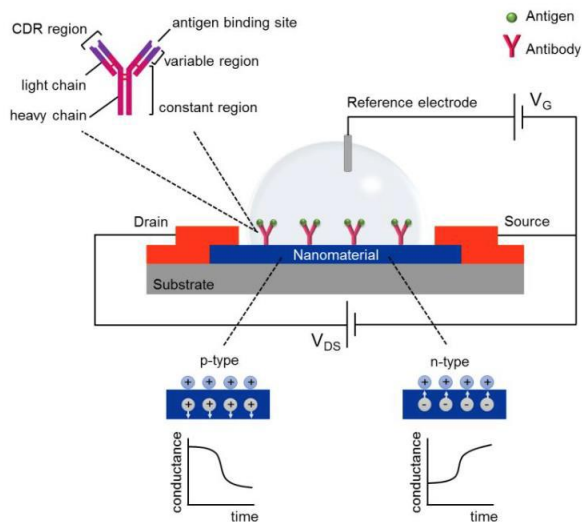


Figure 20. ISFET biosensor [1]

Design of the ISFET device and integration in the sensing chamber

The design of an ISFET device used in the KardiaTool is shown in Figure 21 (all dimensions are expressed in micrometres). The central gate area has a size of 400 x 20. The lateral source and drain areas (green rectangles) have sizes of 400 x 505. This gives a total device size of 400 x 1030.

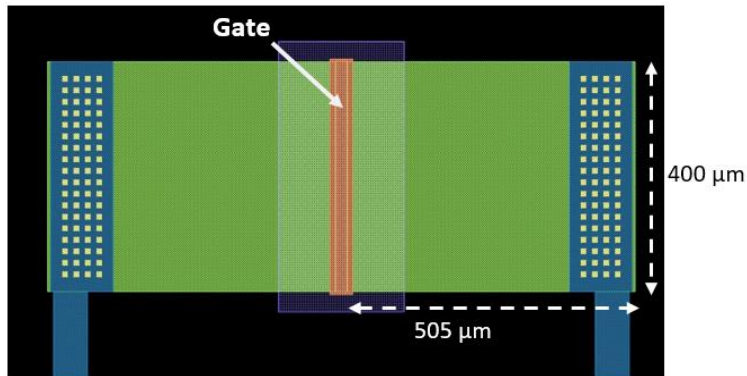


Figure 21. Design of the ISFET device integrated in the KardiaLOC

4.8. Electromagnetic chamber and Magnetic coils

Planar spiral coils are commonly used in industry as radio frequency inductors in integrated circuits to help satisfy the requirement of an high quality factor Q at high frequencies [29]. Usually, they are air-copper coils with a maximum copper thickness of 5 micrometres. The planar coils used in the KardialOC device will be made with a thicker copper and a magnetic core will be used to enhance the cycles of capture and mixing [1]. The partner team responsible for the integration of the magnetic coils in the device evaluated different types of coils in order to find the most efficient design for each coil and array configuration. Single rectangular spiral, double spiral, circular spirals and toroid coils were design tested with the support of finite element modelling software, and the definitive design chosen for the implementation is presented in the following paragraph. Once fabricated, the coils will be protected by a special coating used both to isolate the materials from the wet environment and to ensure that the processes of capture and release are performed efficiently. In Figure 22 is presented the design of the magnetic incubation chamber for the handling of biomarkers attached to the MNPs through the manipulation of magnetic field. The mixing, the incubation and the entrapment of the MNPs suspended in the carrier solution will take place in this chamber. In the electromagnetic and incubation chamber the coils in the array are activated sequentially, causing a fast changing magnetic field in the chamber that agitates the MNPs and enhance the interaction with the biomarkers suspended in the solution. Different coil excitation patterns are developed and tested in order to optimize the biomarker and nanoparticles mixing. When the mixing and the incubation process are completed, a magnetic field with constant amplitude is produced by the magnetic coil array that is powered up, and this newly generated field entrap the MNPs that are activated with the biomarkers on the bottom of the chamber and allows for a fresh rinse solution to flow through the chamber to clean it from the previously introduced suspensions. The magnetic force generated by the coils is sufficient to minimize the loss of activated biomarkers during the rinse cycle. Once the rinse process is completed, a fresh buffer solution is flown through the magnetic chamber. After this step, the activated nanocarriers are released from the bottom of the chamber by turning off the power of the coil arrays. The magnetic force applied to the MNPs can be simplified assuming no interaction among the particles, and is given as:

Where V is the volume of the MNP, X_m is the magnetic susceptibility per unit of volume, H is the strength of the magnetic field and B is the magnetic flux density. For MNPs with fixed values of V and x_m , the magnetic force applied on them depends on the strength of the field and the field gradient. These 2 parameters are the ones that are taken into consideration during the design of the planar coil array. The strength of the magnetic field is limited by the miniaturization of the coils but is compensated by the increasing of the excitation current and by the number of turns per coil. The gradient of the field is controlled and optimized by the coil topology and the overall array design. The coils are made of electroplated copper in order to maximize the electric current and maximizing the induced force. In the following paragraph, the definitive coil design is introduced.

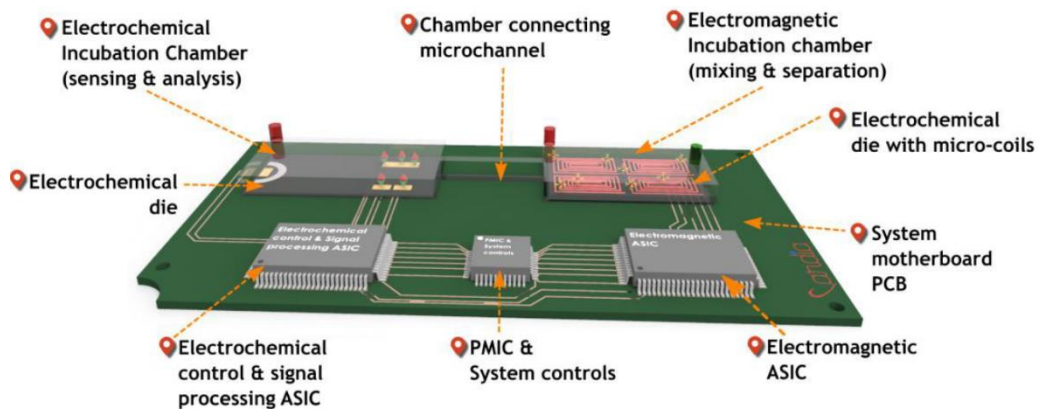


Figure 22. Magnetic incubator chamber designed for the handling of biomarkers attached to the MNPs

Electromagnetic chamber and coils design:

The definitive design for the electromagnetic coils consisted in a linear 1x4 coil array. The advantages of this configuration are multiple:

1. The surface area is small and the chip fits perfectly in the magnetic chamber.
2. The driving current is low, and the temperature increase due to the flow of the current is acceptable, around a 15C temperature rise from the simulations.
3. The design is optimized to work in a “static” mode (no fluid flow) and “dynamic” mode (continuous flow).
4. A magnetic core can be used optionally to improve the field directionality, enhancing the magnetic forces present in the chamber.

5. Sensor integration

In this chapter the methodology and the results of experiments performed for the sensor integration part in the KardiaTool framework are described and reported. The scope of the tests was to define a protocol with appropriate parameter to integrate the two silicon chips (the ISFET chip and the EM chip) inside the LOC environment. The first paragraph of the chapter will describe the theory behind the integration of sensor into a polymeric substrate and provide some example relative to established integration techniques in the biomedical field. The second paragraph will describe the equipment and the material used for the testing of the bonding. The third paragraph will describe the relevant parameter relative to the adhesive glue and the dispensing procedure and how they influence the final result. The fourth paragraph will describe the optimization procedure for the dispensing parameter relative to a specific glue with intermediate characteristics in terms of viscosity. The fifth paragraph will describe the adaptation of the parameters to the other glues that were tested, and the adjustment used to obtain an optimized result for the different kind of glues. The final paragraph will describe the bonding tests performed with fluorescent dye used to assess the hermeticity and the strength of the bonding obtained with the different glues.

5.1. Theory and framework

With the increasing interest in the use of microfluidic for biochemical sensing applications in the recent years, new problem rose related to the integration of different transduction systems based on mechanical, magnetic or electrical phenomena into polymeric substrates. These systems require a direct contact between the transducer and the liquid present inside the fluidic channel to perform the necessary analysis for the system [30]. Transducers are commonly fabricated in silicon due to the amount of established microfabrication processes available for this material and the possibility to integrate electronic circuits in the same substrate with simplicity. The most common solution consists in joining the microfluidic structure and the silicon chip together, one on top of the other and use adhesive or UV glue to seal the bond between them. This results in a hybrid bonding, a bonding between two different types of material, like metal and dielectric. The most common bonding strategies, like anodic bonding, metal diffusion bonding or glass frit bonding are not

compatible with the design and fabrication procedure of the polymeric microfluidic cartridge. The main problems reside in the amount of heat required for the bonding procedure that is too high to be compatible with the materials and the processes employed in the fabrication of a polymeric cartridge [31]. The highest temperature that our system can withstand is 40 degree Celsius, so in this situation the only option available is a low temperature bonding. For the low temperature bonding applied between the elements of the system, the important characteristics are hermeticity to prevent the spilling of liquid inside the system, thermal resistance to withstand the oscillations of temperature in the normal utilization of the device and a good alignment to superimpose the different elements with no mismatch. [32]

The solution that was chosen consisted in the use of UV curable glue as an adhesive between the silicon chip and the polystyrene cartridge. The use of dispensed curable UV glue has been proved to be successful in the framework of microfluidic and biomedical devices and may examples can be found in literature. Use of UV curable resin through interstitial bonding technique has been proved a successful solution for the packaging of microfluidic chip for the separation of DNA strings[32] [33]. The aim of this set of experiment was to find a way to integrate the notions on hybrid bonding present in literature into the KardiaTool framework to obtain an bond between the different components of the Lab-on-chip that is hermetic and durable. For practicality, Figure 24 is the re-proposed the image depicting the assembled LOC:

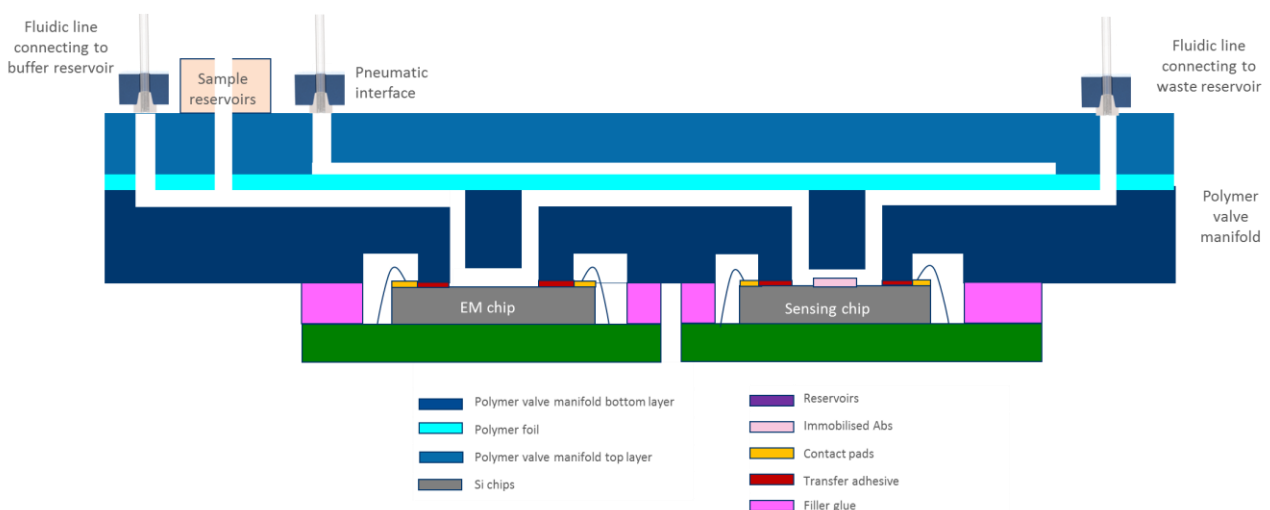


Figure 24. cross section of the assembled Lab-on-chip

As explained in the previous chapters, the polymeric cartridge is installed on a printed circuit board and is interfaced with the two silicon chips, one being the ISFET used for sensing the MNPs and one being the EM chip accommodating the coils. The integration process of the two chips consists in find

the parameters and the appropriate materials (glue/adhesive) to bond the chips to the polymeric cartridge and obtaining a hermetic chamber so that no leak of liquid can come in contact with the contact pads. Figure 25 shows a prototype of the polymeric cartridge where is possible to observe the two chambers, the ISFET chamber and the EM chamber. The two Si chips need to be bonded inside the 2 chambers that are highlighted in Figure 25.

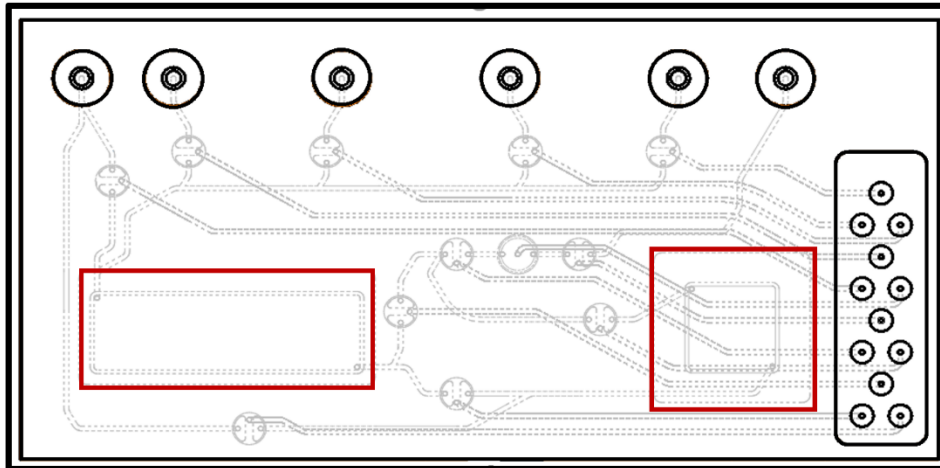


Figure 25. Schematic of the polymeric cartridge with the ISFET chamber (on the right) and the magnetic chamber (on the left) highlighted in red

The initial tests are focused on find a bonding strategy for the integration of the ISFET silicon chip into the polymeric cartridge.

5.2. Materials and equipment

The first step in the integration process consisted in the design of a polymeric dummy cartridge to be used for the different testing sessions. The dummy cartridge was required to be cheap, smaller than the whole polymeric cartridge and easy to dispose. The glue dispensing tests were conducted on those dummy chips to obtain a first set of working parameters, to test the behaviour of the different glues and to measure the difficulty in dispensing liquid glue on the desired surface. The bonding requirements tested with this cartridge were the homogeneity of the dispensing of the glue, the ability to withstand some amount of water or air pressure and a good hermeticity. These requirements will all be tested, and the results will be presented in the last paragraph of this chapter.

Figure 26 shows the design of the cartridge and a mockup bonding configuration with a silicon chip mounted on a PCB. The dummy chip is the reproduction of the ISFET chamber present in the polymeric cartridge and is square shaped with 1-millimetre length and thickness. Two cavities are present in this structure, the external one being 930 micrometres deep and designed to accommodate for the bonding pads connecting the silicon chips to the circuitry. The other cavity, the internal one, is 100 micrometres deep and reproduces the ISFET chamber where the liquid sample comes in contact with the sensing chip. Two circular inlets with 30 micrometre diameters are present on the top of the ISFET chamber and will be used to flow liquid and air inside the chamber after the bonding process to test the strength of the bonding. The two cavities are separated by a wall 250 micrometres thick that will be in contact with the silicon chip and form the walls of the ISFET chamber. The glue or adhesive will be dispensed on this internal wall to form a homogeneous layer and then the silicon chip will be bonded to the polymer. The dummy chip was made in polystyrene, the same material as the polymeric cartridge and is presented in Figure 26.

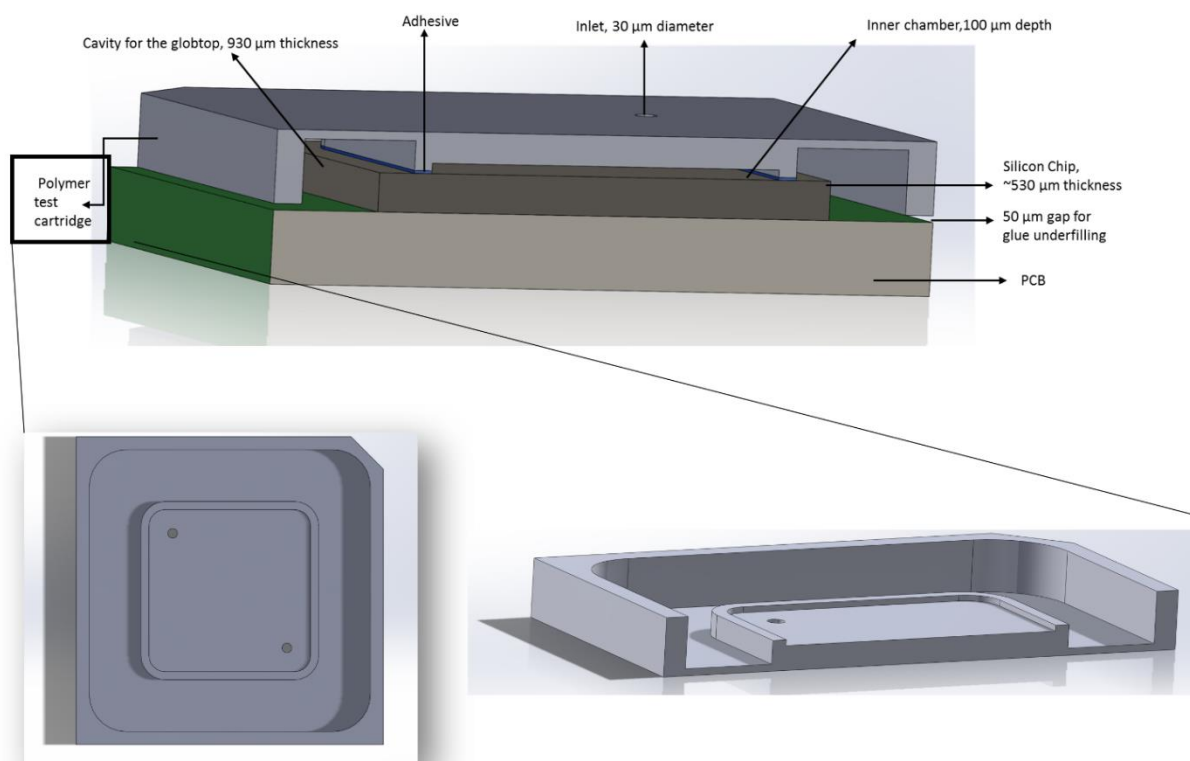


Figure 26. Dummy polymeric chip cartridge

The fabrication was performed with a milling machine and the batch of chip produced consisted in 64 chips from a 130 mm x 130 mm polystyrene substrate and the results is presented in the figure x. All the experiments were performed using the dispense master DD-500 machine. The machine is

a desktop platform that moves the dispense valve in the X, Y, Z direction instead of moving the product on a movable table. A single dispensing valve can be mounted on the machine and so the machine can dispense one glue at a time. The main parameters of the machine can be controlled with a windows based software installed on the computer connected to it, except for the pressure that is controlled with an external turning knob. Using the machine, is relatively easy to dispense the glue precisely in basic geometrical patterns, using lines, circles and dots. The machine can dispense the liquid glues on a maximum surface of 50cm X 50 cm [34]. Figure 27 shows a view of the machine and all its main components, consisting in the main body, the precision moving head connected to the syringe and the test board.



Figure 27. DD-500 dispensing machine

For the dispensing test, initially four kinds of glues were used, and their main characteristics are described in the following sections:

NOA68: Norland Optical Adhesive 68 is a clear, colourless and liquid photo polymer that cures when exposed to ultraviolet light. This glue is designed to produce a good and improved adhesion to many different plastic materials, like acrylics and polycarbonates. The use of this glue eliminates premixing, drying and heat curing operations that are common for the curing of other optical adhesives, allowing to produce low-temperature strong bonding. The curing of the glue is fairly fast and depends of the amount of the UV light energy available and the thickness of the substrate, starting from 5-10 seconds for a 1-5 millimetres layer of glue with a 100 Watt mercury spot lamp positioned at 6 inches of distance to 15 minutes for a full cure of 5 millimetres of glue with a 15

Watt lamp at 3 inches distance. When the glue is fully cured, good adhesion and solvent resistance properties are achieved. The resistance to temperature after aging is also good and the glue can withstand temperature from -80 to 90 degree Celsius and can reach resistance up to 125 degree with the appropriate coating [35]. The viscosity of the glue is 5000 mPa.s at 25 Celsius, a medium value compared to the other glues that were tested.

Dymax 1072-M: The Dymax is a non-fluorescing, flexible medical device adhesive design for rapid bonding of a variety of polymer and plastics like COC or COP. It contains no nonreactive solvents and cure when is exposed to visible and UV light. The curing process is very fast, around seconds, and this enables fast processing with greater output compared to other glues. Also, in this case the depth of the curing process depends on the time of the UV exposition and the intensity of the UV energy beam. The exposition parameters are not far from the one used for the the curing of the NOA 68 glue, needing to expose a 5 millimetre layer of glue for 15 seconds with a 200 W UV lamp to obtain a full cure[36]. The viscosity of the glue is around 1000 mPa.s and is one of the lowest viscosity glues that were tested.

PERMABOND UV632: Is a UV-curing adhesive developed specifically for use on plastic and it cures to give a colourless bond. It has a very good adhesion to acrylic and the photo initiators present in the glue reacts to a wide spectre of wavelength, allowing for a curing process even through plastics that are UV-stabilised. This glue is used to cure plastics, glasses, metals and other materials. The time of the curing process depends on the power of the UV lamp, its spectral output, the distance between the lamp and the plastic component and the transmission characteristic of the plastic substrate. The curing process is fairly fast, even compared to the curing processes of the other glues, needing only 2 seconds for a 5 millimetres deposition with a UV light guide with 20W/cm² [37]. The viscosity at 25 degree Celsius is 200-400 mPa.s, and this viscosity is the lowest of all the glue uses in the testing process.

IQ-BOND 8419 UV: The IQ bond is a UV-curable, solvent free acrylic based adhesive, developed for optical applications, structural bonding applications and wire-fixing on circuit boards. Typical applications include bonding of glass and metals, but the glue is employed also in applications where a flexible and humidity resistance is required. As for the previous glues, the time and the dose required for a full curing depends on the thickness of the glue layer, the intensity of the UV emission as well as the UV transparency of the substrate [38]. In this case, for a glue layer of 5-millimetre thickness, the time required for a full cure ranges from 30 to 60 seconds and the power of the lamp

necessary for a full cure range from 2000 to 5000 mW/cm². The viscosity of the glue is equal to 20.000 mPa.s, and it is the highest viscosity among the glues chosen for the testing.

The glues were chosen to cover a wide spectrum of viscosities to identify the relevant differences in the curing and in the bonding process, and the lamp used was a 200 W UV lamp with an emission spectrum of 480 nm. All the samples were cured for 1 minute, to be sure that the glue layer was fully cured in its entirety.

5.3. Dispensing test parameters

The process of dispensing is affected by many different parameters, some inherent to the properties of the single glue and other relative to the setting of the machine. In order to obtain a uniform distribution of glue is important to know how the parameters influence the deposition process and how to change them to obtain the optimal results. In this section the influential parameters are all described in detail and related between each other to see how the change on a single parameter can affect the final result.

Viscosity of the dispensed glue: This determine how easy the dispensed fluid flow; a high viscosity means that the fluid flows very slowly from the dispensing syringe. The viscosity also limits the minimum diameter of the needle with the glues having higher viscosity needing a needle with larger diameters. The diameter of the needle and the viscosity of the glue are intercorrelated parameters, and to each range of viscosities is assigned a different needle.

Temperature of the working environment: The temperature of the working environment is one of the least influential parameters, but it still needs to be considered. The temperature influences the viscosity of the dispensed glue and needs to be kept as constant as possible to have a high reproducibility rate for the different dispensing sessions.

Needle diameter and length: The maximum diameter of the needle acceptable for the test is determined by the surface on which the fluid must be dispensed and by the viscosity of the dispense fluid. The needle diameter must be put into correlation with the viscosity of the glue, if the needle is large and the glue has a low viscosity the glue flows from the needle and the dispensing produces and overflow and if the needle has a small diameter and the glue has high viscosity the dispensing process is non-homogeneous. The length of the needle is another important parameter that has to

be taken into account. If the viscosity of the glue is too high, a long needle combined with a small diameter can cause the dispense fluid to stick in the needle.

Height of the needle: The height of the needle refers to the distance between the tip of the needle and the surface where the machine dispenses the glue. This is the most problematic parameter to set and the one that fluctuates the most between the experimental sessions, since the configuration of the position of the needle is done manually. The needle is lowered to the point it touches the surface of the material, the position is registered by the system and during the dispensing the needle is raised from the surface with a pre-defined height, usually 50 or 100 micrometres.

Applied pressure: This parameter refers to the pressure that the system applies the glue syringe during the dispensing procedure. This parameter affects directly the amount of liquid that is dispensed and needs to be changed depending on the viscosity of the dispensed glue. The more pressure is applied, the more liquid is dispensed.

Motor speed: This parameter refers to the speed of the needle while following the dispensing path during the dispensing procedure. This parameter affects directly the amount of liquid dispensed and is more and more relevant the more the dispensing path is complex. If the other parameters are kept constant, more glue is dispensed in a dispensing session the slower the needle follows the dispensing path.

Dispense time: This parameter refers to the beginning and ending in time of the dispensing procedure. Is possible to set when the machine starts and ends the dispensing of the glue in relation to the beginning and the end of the motion of the needle. Is useful to set the machine to start applying the pressure slightly before the beginning of the movement of the needle to be sure to dispense along the whole dispensing part and finish applying the pressure slightly after the stop of the needle.

All these factors influence each other can be tuned to compensate the effects of the others. For example, is possible to use a large needle diameter and set the pressure to a lower value to obtain a dot of the size equal to the one obtained with a smaller diameter needle with a higher applied pressure.

5.4. Optimization of the parameters for the deposition of a single glue

The aim of the test was to identify a set of parameters resulting constantly in a uniform deposition of glue along the desired part, with no missing spots and no overflow of liquid into or outside the inner chamber of the dummy cartridge. The following set of images present the results obtained with the four different glues. The different steps of dispensing, bonding and curing are presented, and the optimization of the different parameters towards an optimal result is highlighted. The idea behind the test is the application of an iterative process, with modification of the parameters until the optimal result is achieved. The first set of parameters is applied knowing the guidelines present in the dispensing machine user manual, that introduce standardized parameters in relation to a glue of medium viscosity. The result is analysed, and the set of parameters is further modified.

NOA68

The first tests are performed with the glue NOA68 whose viscosity is average compared to the other glues used in the test, 5000 mPa.s. Initial parameter set up for the dispensing were: 25-gauge needle, 8 mm/s needle speed, 1.5 bar pressure, and 50 micrometre needle height in an environment with controlled temperature of 24 degree Celsius. These were the average parameters suggested in the dispenser user manual guidelines for a glue with medium viscosity. The results of this first test are presented in Figure 28 A. It is immediately possible to see that the results are far from an optimized result. The glue is not dispensed homogeneously along the length of the wall and there are sections of the wall where the glue is not dispensed at all. Moreover, in the upper section of the wall there is an overflow of glue due to the accumulation and release of liquid on the tip of the needle during the movement of the dispensing machine. The problematic parameters that led to these results are identified to be the pressure, that is too low and to achieve a homogeneous deposition and the dimension of the needle, that is too big and causes the overflow of glue from the walls.

The experiment was repeated while changing needle, using a smaller 25 gauge one and increasing the applied pressure to 3 bar. The results of the tests are presented on Figure 28 B. The glue is dispensed more homogeneously, and the layer of glue is almost uniform along all the wall dimension. It is still possible to notice the presence of 2 spots along the path of the wall where the glue was not dispensed properly. To correct this problem and obtain a more uniform result, the

speed of the needle was decreased from 8 mm/s to 7 mm/s, in order to increase the amount of glue dispensed along the path. Figure 28 C shows the final results of the tests with NOA 68 glue

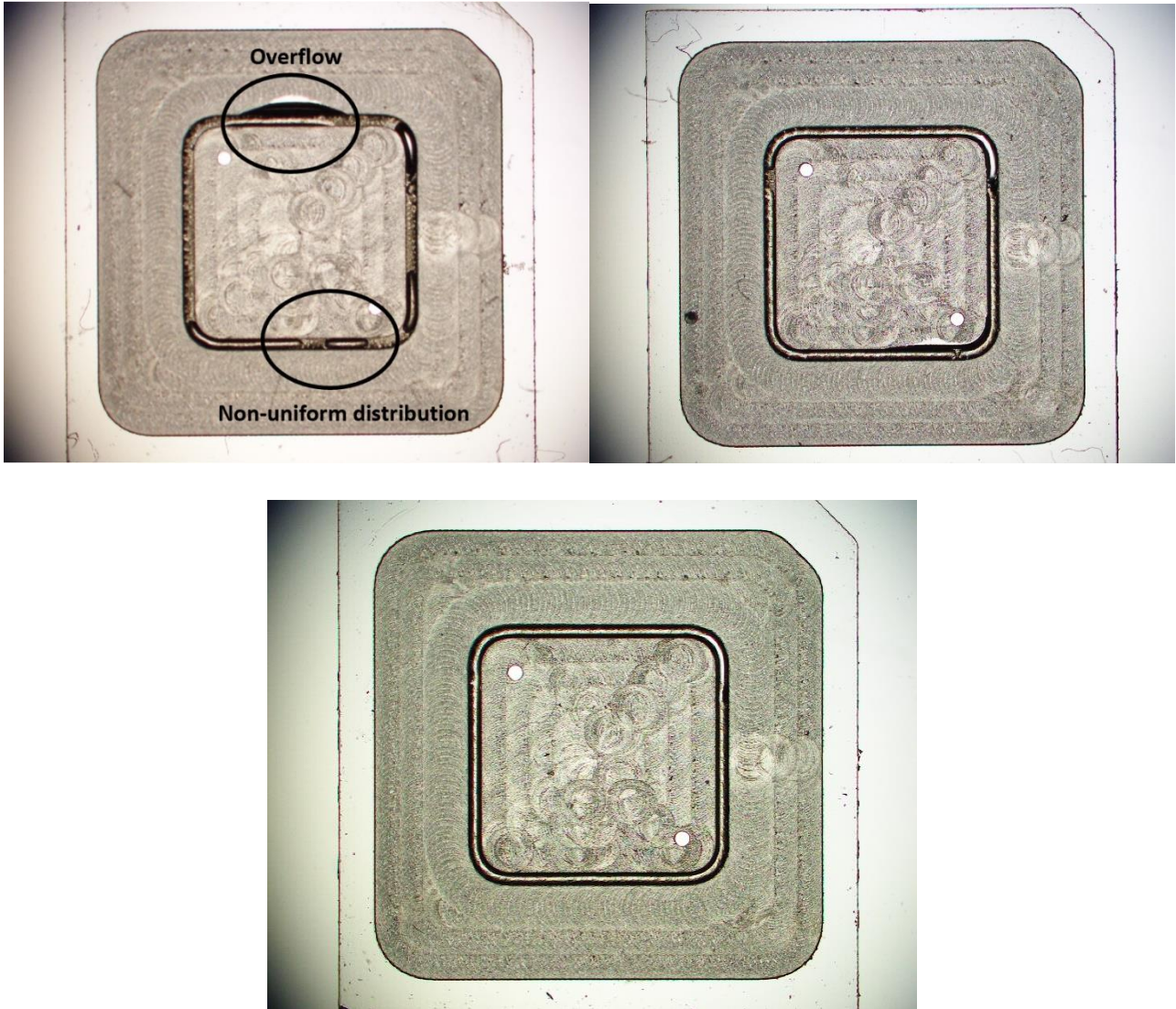


Figure 28. Results of NOA68 glue dispensing. A) dispensing of the glue with non-optimized parameters, overflow and non-uniform distribution of glue are present. B) distribution of glue with optimized parameters. It is possible to notice that the glue is not perfectly uniform. C) distribution of glue with definitive parameters

After the dispensing process, the sample is bonded to a piece of glass slide, cut to fit in the chamber. The bonding tests were done with glass slides since is an inert material useful to be used as model. Figure 29 A) depict the glass slides on bonded to the chip before the curing process while Figure 29 B) depicts the sample after the curing process, consisting in 1 minute's exposition to UV lamp with power of 200 Watts.

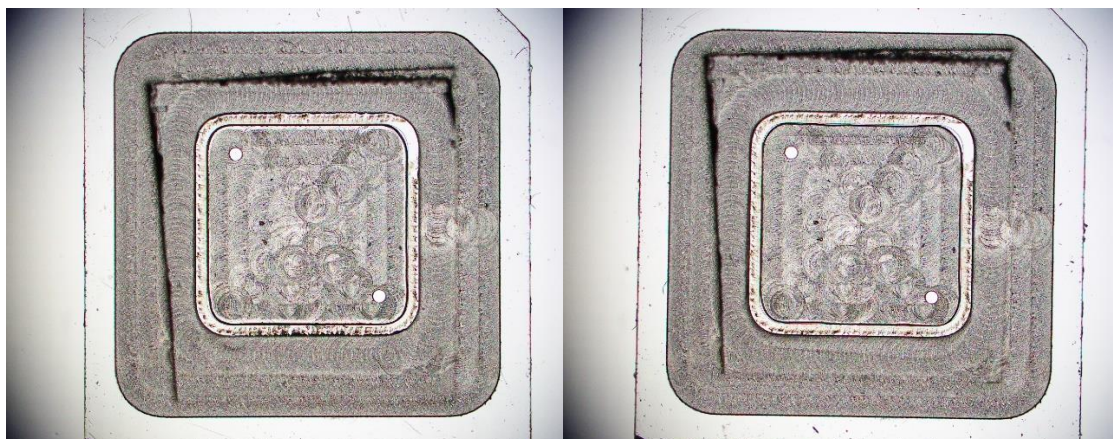


Figure 29. Dummy chip after the processes of deposition and bonding with a piece of glass slide

The bonding obtained after the curing process was resistant, and withstood some amount of mechanical pressure. A better characterization of the bonding strength will be performed in the final paragraph of this chapter. The results of the test with the glue NOA68 were optimal and the objective of finding parameters to obtain a uniform deposition of glue on the 250 micrometre thick walls.

5.5. Optimization of parameters for glues with different characteristics

This paragraph describes the methodology behind the optimization of the parameter of the testing with glues with viscosities different from the average one of NOA68. The parameters are the same that were introduced in the previous paragraph, and the different steps and the optimized result will be presented through images

Dymax 10-72

The Dymax 10-72 is a low viscosity glue with a viscosity of 1000 mPa.s. The first test is performed with the same initial parameters of the NOA68 tests, but in this case the applied pressure was chosen to be lowered to 1 bar in order to prevent overflow of glue due to the low viscosity. The result of the first test are presented in figure Y. Unfortunately, there is still a huge overflow present after the dispensing session and that was identified to be related to the dimension of the needle. The first optimization of the procedure involved the reduction of the diameter of the needle from 25 gauge to 30 gauge. All the other parameters were left unchanged.

The test continued with the optimized parameters and the results can be observed in Figure 30. In this case, the deposition of glue on the walls present no overflow and a good uniformity. This set of parameters was tested multiple times, and the results proved to be consistent for this low viscosity glue.

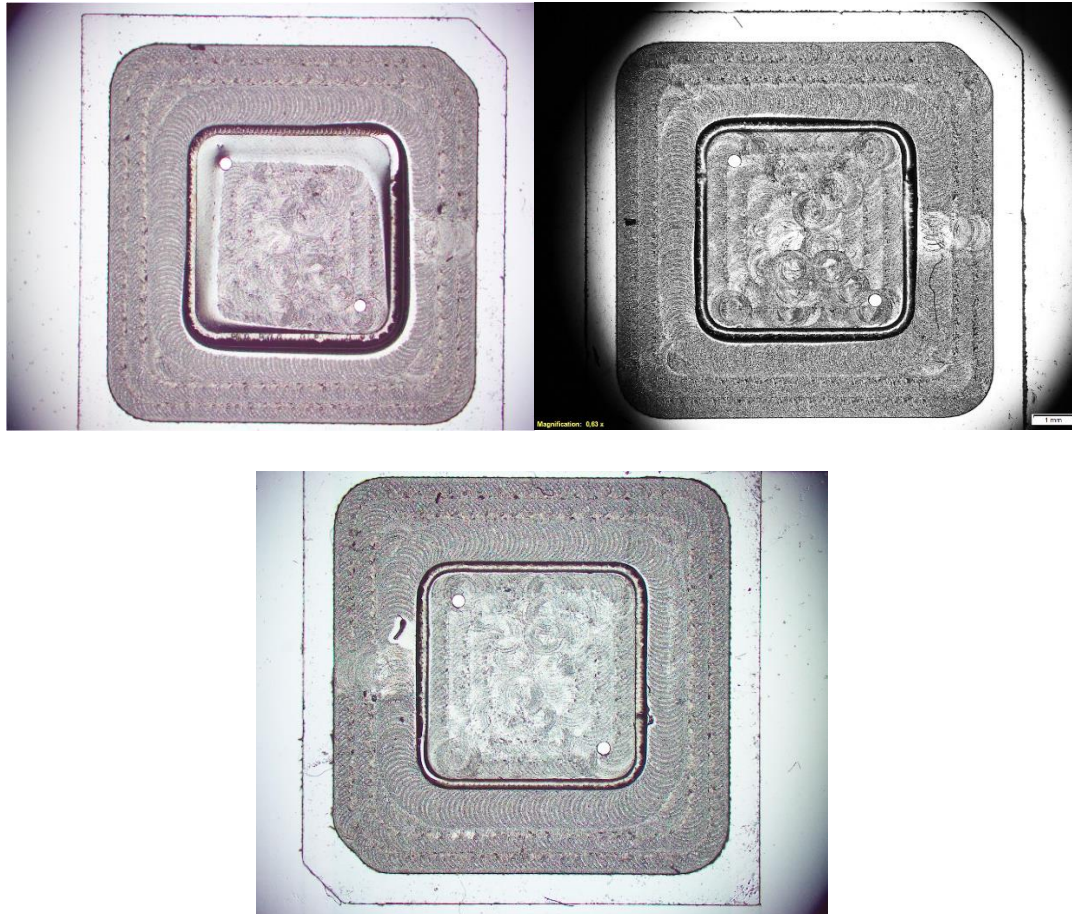


Figure 30: Results of Dymax glue dispensing. A) dispensing of the glue with non-optimized parameters, huge overflow is present due to the low viscosity of the glue. B) distribution of glue with optimized parameters. Is possible to notice that the glue is not perfectly uniform. C) distribution of glue with definitive parameters

Permabond 630

The Permabond was the third glue that was tested, and the one with the lowest viscosity among the batch of glues, 200 mPa.s. In this case, the parameters used for the first test were the ones obtained from the test on the Dymax 10-72M. The only parameter that was changed was the pressure, that was lowered to 0.5 bar to compensate for the difference of viscosities among the 2 different glues. The results of the test with these parameters can be observed in Figure 31. The deposition presents no overflow and a good degree of homogeneity, demonstrating that this set of parameters can be used for glues with similar characteristics of viscosity

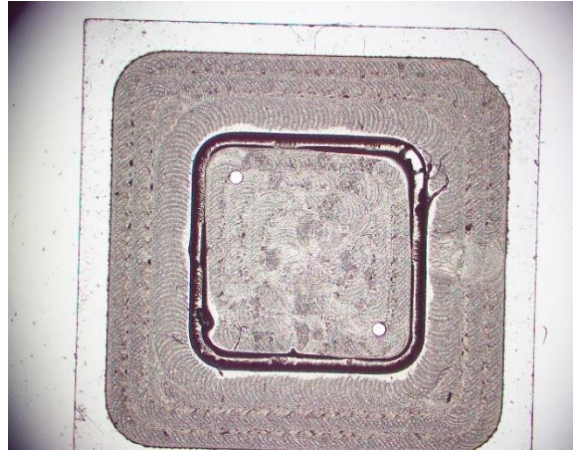


Figure 31. Dispensing results obtained with Permabond glue with parameters adjusted from previous experiments. The deposition is acceptable with non-optimized parameters even in the glue is not homogeneous since there is no strong overflow

IQ-BOND 8419 UV

The IQ-BOND 8419 UV is the last glue that was tested and is the glue with the highest viscosity. In this case the test started with the parameters of the NOA 68. The following tests were performed modifying the most influential parameter for a high viscosity glue, the external applied pressure, that was raised to 4 bar. The result is presented in Figure 32, and it presents an acceptable degree of homogeneity and no overflow, with no spots where the glue was not dispensed. Due to the high viscosity of the glue, there are some parts of the deposited layer that are thicker in comparison to the average thickness. Even in this configuration, the glue does not overflow and the final deposited layer is acceptable.

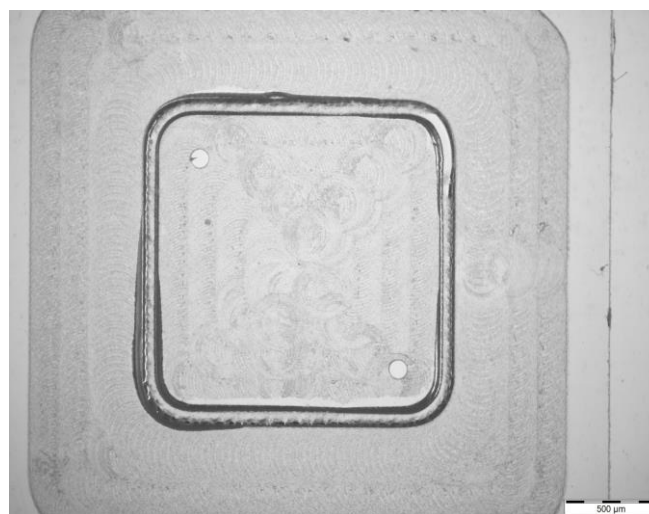


Figure 32. IQ-BOND 9419 UV glue test dispensing.

With this last test, all the different glues were tested and a set of parameters able to obtain an optimized result was extracted for all of them. These optimized parameters are summarized in the following table

Glue	Viscosity [mPa.s]	Temperature [C]	Needle Dimension [gauge]	Height [mm]	Pressure [bar]	speed [mm/s]	Dispense time [ms]
Permabond 630	400.00	24.00	30	0.05	0.50	8.00	+100; -100
Dymax 10- 72 M	1000.00	24.00	30	0.05	1.00	8.00	+100; -100
Noa68	5000 .00	24.00	30	0.05	3.00	7.00	+100; -100
IQ-BOND 8419 UV	20000.00	24.00	25	0.05	4.00	8.00	+100; -100

5.6. Bonding strength and hermeticity tests results

Once the samples were bonded with a glass slide and cured, the polymer-silica seal was tested for hermeticity and resistance to liquid pressure. Fluorescent dye was pumped in the chamber through one inlet, the sample was left to rest for 5 minutes allowing the fluid to flow through the possible leaks in the bonding and the result was then observed through fluorescence microscopy. Figure 33 present the results obtained for two glues, the NOA 68 and the Dymax. In all cases can be observed that no leaks are presents, and the bonding between the polymer and the glass slide is hermetic and liquid proof.

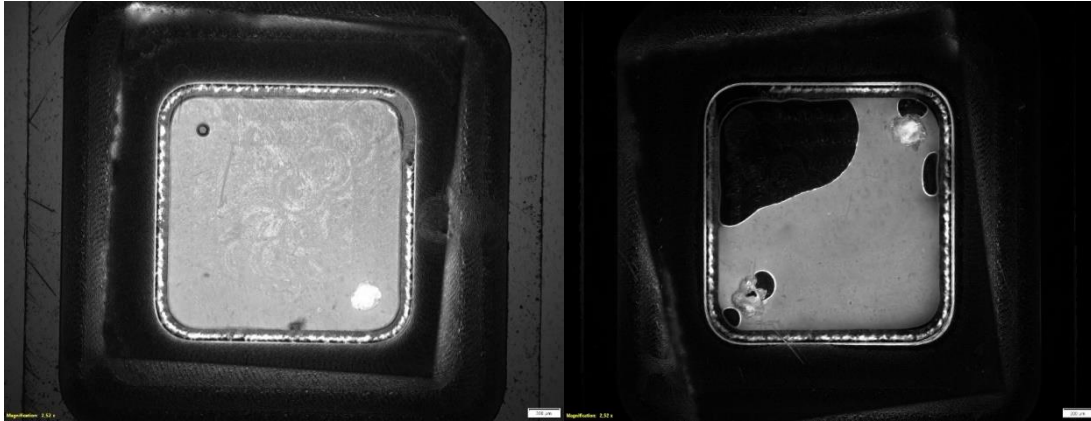


Figure 33. NOA68 bonding fluorescence test result. A) The fluorescent dye does not leak through the bonding connections, and completely fills the chamber. B) Same instance as in figure A), but some air is trapped inside the chamber. The bonding is still hermetic.

For the different glues, no leaks were observed, and the final bonding obtained with the different parameters was judged hermetic.

5.7. Considerations on the testing results

The testing of the glue was considered successful for this first stage of work. The results consisted in the capacity to dispense different kind of glues with a wide range of viscosities on the wall of the dummy chip with good localization, and in these cases the glue remained localized after the contact with the glass slide, with minimum overflow of glue in the internal chamber. Moreover, the hermeticity and the resistance of the bonding to pressure and liquid flow was tested, and all the test were successful, confirming that the glues that were identified can be used in further testing session with the definitive polymeric cartridge.

The next part of the work in the sensor integration for KardiaTool will consist in performing bonding test with materials with different surface energy from glass, near the surface energy of the functionalized substrate that will be used in the assembled device, like Si_3N_4 and HfO_2 . Integration tests are also to be performed with the whole microfluidic cartridge as a substrate, finding a way to stabilize the bonding on a wider surface and trying to assess quantitatively the strength of the bonding.

6. Microfluidic chip testing and characterization

6.1. Introduction and methods

After performing the tests on the integration of the silicon sensors, the Micronit team moved on the fabrication and testing of the polymeric cartridge. The different parts of the work consisted in the adjustment of the initial design, the fabrication and the characterization of the polystyrene polymeric cartridge for the KardiaTool lab on chip. In this chapter some insight on the design and fabrication procedure are presented and the results of the different characterization tests performed on the various batches of chip produced are described. Once the first prototype cartridge was successfully fabricated the following step in the workflow was to test the behavior of the different valves and the efficiency of the pumping system. The microfluidic device was tested using an external software controlling the pneumatic interface through a system of pressure pumps. The system could apply a positive pressure of up to 2 Bar and a negative pressure up to -0.6 bar to all the different valves independently, to actively open and seal them shut. The system was also used to control the actuation of the internal pumping system, consisting in three adjacent valves that are opened and closed at a pre-defined rate. Tanks filled with liquid were connected to the microfluidic network of the cartridge and the flow through the valves toward the waste tank was measured and observed. All the parts of the microfluidic chip were tested independently to assess the optimal functioning and a pumping behavior coherent with the theoretical expectations. The first paragraph will explain how the microfluidic valves present inside the chip were characterized using optical and fluorescence microscopy, the second paragraph will describe the characterization of the working behavior of the microfluidic chip, the third paragraph will describe the tests on the complete working assay and the priming optimization.

6.2. Microfluidic valves characterization

The first step in the characterization procedure was to assess the behavior of the microfluidic valves, the ones used to control the flow in the chip and the ones used to generate the internal flow of the liquid. Different methods were employed to observe the behavior of the valves. First, the deflection of the membrane was observed through optical microscopy and pure water was used as liquid medium. To improve the contrast, the clear water was then substituted with blue dyed water. After that, the valves were tested through the use of a fluorescent dye, to observe the presence of eventual leaks of liquid through the membrane and to try to give a spatial representation of the behavior of the membrane in volume of the valve.

6.2.1. Valve operation

The first step of the characterization process consisted in the assessment of the functionality of the valves of the chip. The valve functionality is verified by demonstrating if it can prevent fluid flow when closed and allow it when opened. For such a demonstration the pump is constantly running, and two liquids are used: PBS stained with a blue dye and PBS (colourless). Valves are alternately closed and opened to induce an alternate flow of the stained and unstained solution. An example of operation is depicted in Figure 34.

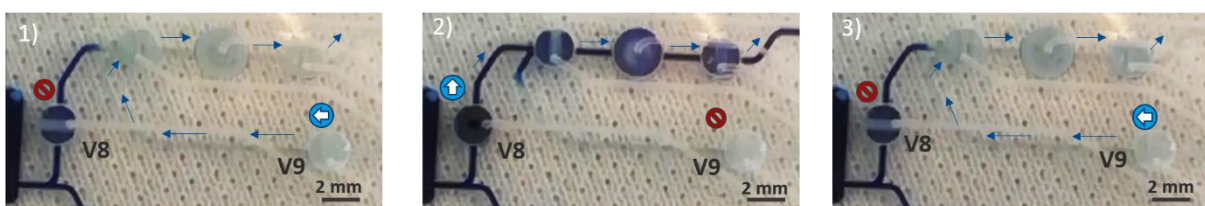


Figure 34. Pictures of an example of a test sequence for validating a valve functionality.

In this example the proper closing and opening of valve #8 is tested. First, the valve V8 is closed while valve 9 is opened, allowing the colourless liquid to flow (Figure 34.1). Then, valve 8 is opened while valve 9 is closed, allowing the blue-dyed liquid to flow (Figure 34.2). Eventually, valve 8 is closed again while valve 9 is opened, allowing the colourless liquid to flow (Figure 34.3). A general overview of the results for the functionality of the valve for the different batch of the chips is presented in the next paragraph.

6.2.2. optical characterization of the microfluidic valves

In this section are presented the results relative to the initial characterization of the microfluidic valves through optical microscopy. The valves of a chip were observed during the actuation of the microfluidic pump, and attention was paid to the movement of the membrane. In Figure 35 is presented a valve from the first batch of chip in the two different actuation states: In Figure 35.a) the valve is in open state, while in Figure 35.b) the valve is closed. When the valve is closed, is possible to see the shadow of the membrane, indicating a deflection from the idle state. However, even if some information can be extracted from these typologies of testing, the contrast is too low, and no information are obtained on the degree the membrane is closing the microfluidic channel and how much the seal is hermetic.

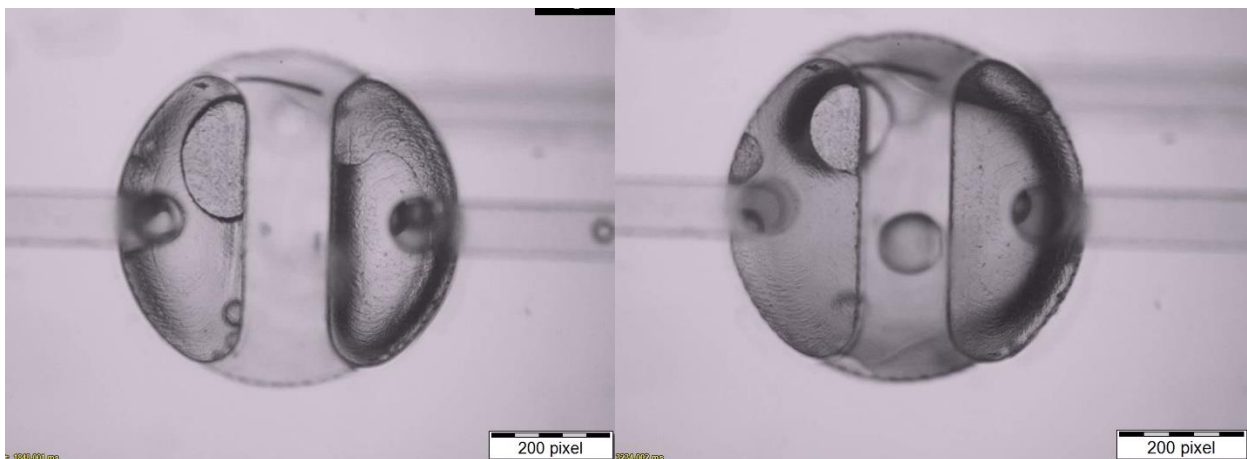


Figure 35. Valve observed through optical microscopy. 32.a) Valve in open state; 32.b) Valve in closed state

To increase the contrast and obtain more detailed information on the behavior of the membrane, the test was performed with the use of fluorescence dye performing fluorescence microscopy.

6.2.3. Fluorescence testing

In order to find a way to characterize with an improved contrast the movement of the middle membrane of the valve during actuation, the behaviour of the device was observed through fluorescence microscopy. The fluorescent dye used was a solution of calcium fluoride, concentration of 1 mg in 100 ml of water. For this test, the aim was to obtain clear images and a 3D models of working valves to have a database that could be used to compare the results of fluorescence tests performed on the different batches of chips, both functional and not functional ones. The first images were obtained by flowing the fluorescent dye through completely functioning valves, meaning valves that managed to stop the flow of the fluid when closed and offered low to zero resistance to the fluid when open. The working set-up consisted in an optical microscope equipped with an UV lamp able to excite the fluorescent dye. The light emitted from the sample was collected by the microscope and analysed through a software. Different parameters were tested in order to find the optimal setting for the observation of the fluorescent dye, and they were set to a value ideal for the observation of the dye in the channel and in the valve with a good contrast. The final set of parameters chosen for the observation of the samples was the following: Exposition time: 50 ms; gain: 1 DB; gamma: 1,3; sharpness 15; contrast 1,1; brightness 0; All the images were taken as 8-bit images in grey scale and analysed through the program IMAGEJ. Figure 36 presents some of the valves that were observed with the optimized parameters.

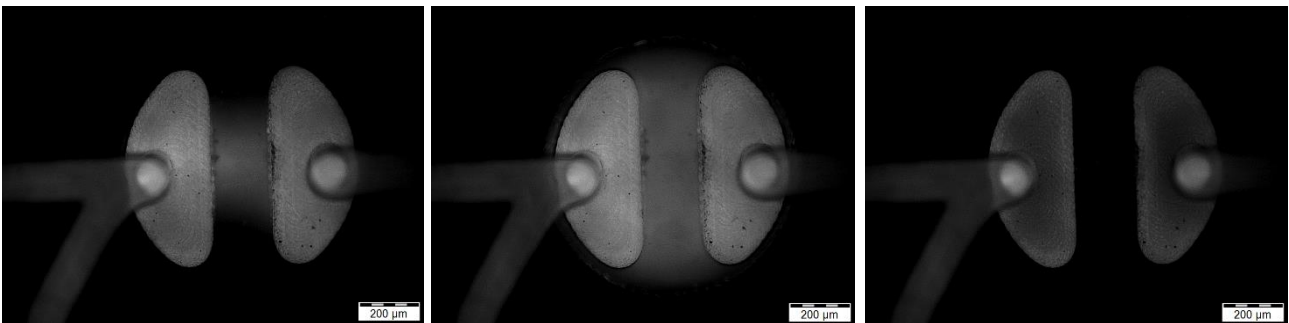


Figure 36. Observation of valves through fluorescence microscopy: 33.a) valve in idle state, 33.b) valve in open state, 33.c) valve in closed state

The valve analysed in this test was the valve 11 of the third chip from the second batch of chips. The valve was completely functional and will be used as standard for the analysis of the behaviour of the other valves. Figure 36 shows the 3 possible states of a microfluidic valve: Idle state, open state and closed state. In the idle state, no pressure is applied to the valve and the liquid can flow if the fluidic pressure is higher than the atmospheric pressure; in open state negative pressure is applied

up to -0.6 bar and in closed state positive pressure is applied to the membrane up to 2 bar.

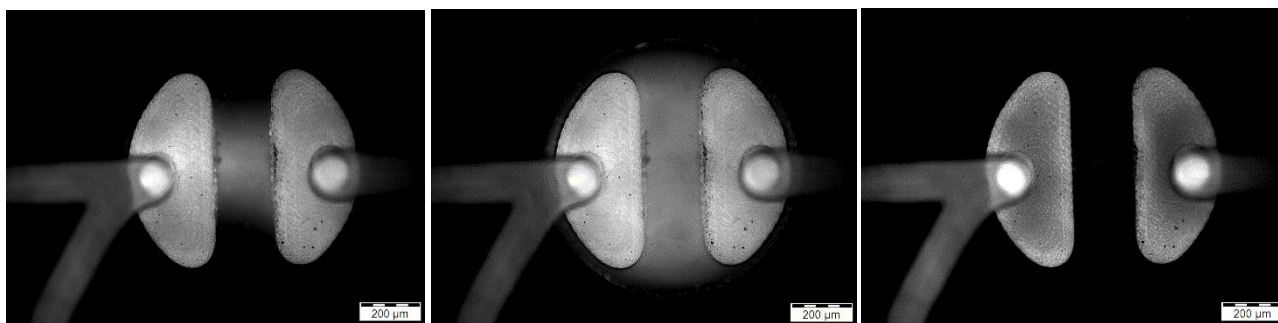


Figure 37. Modification of image parameters of figure 33 through the software IMAGEJ

These images are analysed employing the software ImageJ. The first step in the treatment of the pictures consisted in the adjustment of display range of the LUT (Look up table). In 8-bit images, to each pixel is assigned a value that characterizes the brightness of that pixel, ranging from 0 to 255. The adjustment of the values of the pixels was performed through the software ImageJ and consisted in the reduction of the threshold determining the maximum effective brightness in the image obtained after the analysis of the software. So, to the pixel which contained the maximum brightness value the maximum effective brightness value was assigned, and this brought to a final image in which the whole range of brightness pixels were used. The result of this first modification of these images are presented in Figure 37. As said before, the values of the pixels in these images are scaled so that they occupy the whole possible brightness spectrum for a pixel in an 8-bit image. In this configuration is simpler to observe the distribution of fluorescent dye in the valve since the contrast of the image is enhanced. In this case, for example, is easier to judge the behaviour of the membrane as a seal when it is in closed state, since the image clearly does not show sign traces of fluorescence dye under the closed membrane. Through the use of fluorescence dye, it was possible to assess the hermeticity of the membrane seal in closed state.

Relevant results from the fluorescence analysis

With the setting described in the previous paragraph, the valves from chips from different batches were analysed to observe the behaviour of the membrane and relate it to the production parameter. In this paragraph are presented some relevant membrane behaviour observed through the testing sessions.

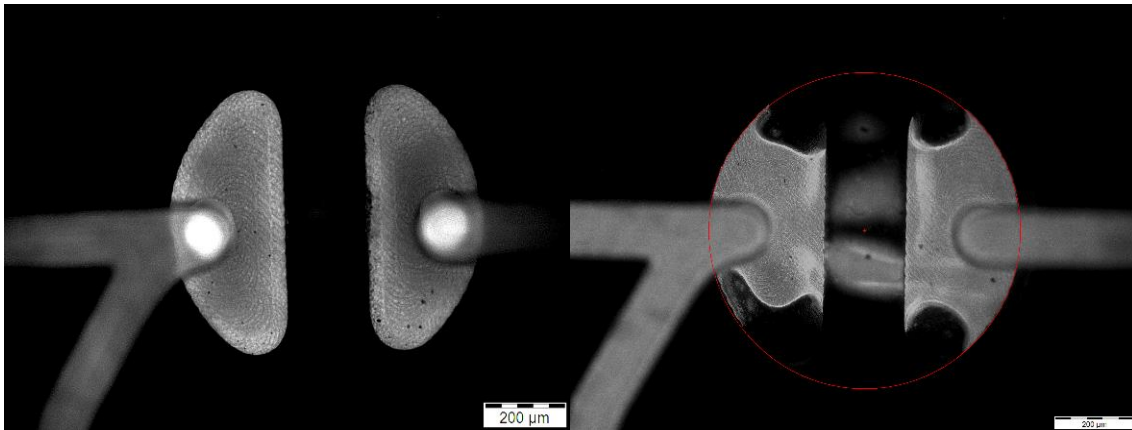


Figure 38. images of a functional and a dysfunctional valve. 3.a) presents a fully functional valve in closed state; 3.b) presents a malfunctioning valve and is possible to observe leaks through the pneumatic seal

In Figure 38 are presented two images obtained from two valves part of chips coming from the second batch of production. The figure on the left introduces a completely working valve while external pressure is applied: The pixels present at the centre of the membrane are completely dark, confirming that the membrane is sealed shut and no fluorescent dye can pass through even when there is applied fluidic pressure. The figure on the right presents instead a malfunctioning valve in closed state: Is possible to observe that the membrane is not perfectly flat at the centre, introducing some corrugations where the fluorescent dye can flow and accumulate. This non optimal behaviour of the thermoplastic membrane of the valve can be attributed to the presence of defects during the fabrication procedure; in this particular case, the production team reported that the temperature used during the bonding process was non-optimal and the membrane was not tense enough during the bonding of the two different layers. These errors brought to the malfunctioning of the microfluidic valve while in closed state. Other relevant results came from the analysis of the valve behaviour from the third batch of microfluidic chips: This batch consisting of eight chips had a yield of 0, due to the behaviour of the membrane of the valves that was not deflecting. There were two initial hypotheses about the behaviour of a non-actuating membrane. In the first theoretical configuration, the membrane is fully attached to both the walls of the inner chamber and its upper part and it is impossible to detach and make it flex. In the second theoretical configuration the membrane is not directly attached and adhere to the walls and the top of the chamber but is partially bended inside the chamber and made plastic and non-bendable during the production process (errors in parameters). The behaviour of these membrane was observed to assess which of these hypotheses was the most fitting one. Figure 39 introduces one of these valves in idle state. Is observable that although no external pressure is applied to the membrane, the amount of fluorescence dye and the brightness is comparable to a functioning valve in open state and not in

idle state. Independently from the amount of pressure applied to this valve, no changes in the brightness of the image are detected during the testing session, meaning that the valve was completely in a plastic state after the fabrication process and any kind of bending is impossible. The results were communicated to the production team to improve the results for the future produced batches.

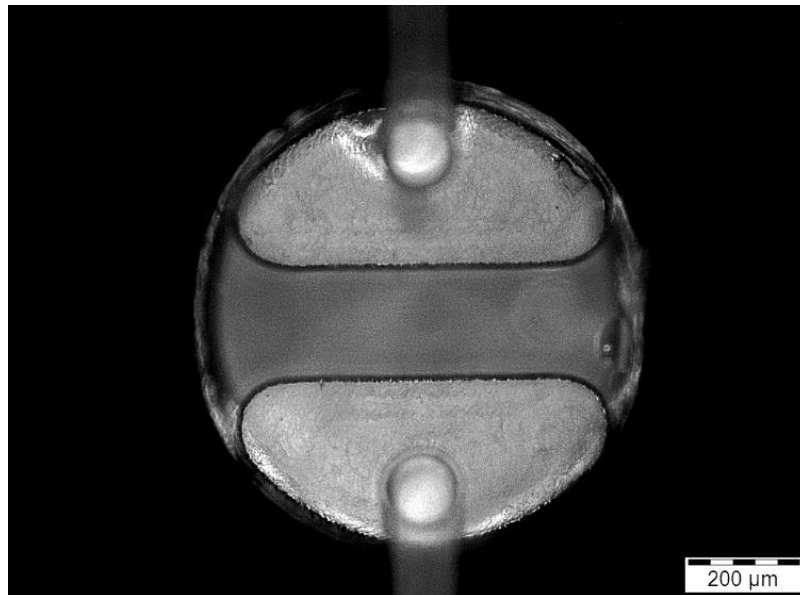


Figure 39. observation of a blocked valve from the third chip batch. In this valve, the membrane does not deflect independently from the pressure that is applied

An example of plastic behavior of the membrane can also be observed in Figure 40, where the membrane is also heavily deformed. The amount of liquid present under the membrane is comparable to the amount present in the valve in Figure 39 since the brightness of the pixels is comparable, but in this case the membrane is not completely open at the edge, and is instead corrugated and stuck at the edges of the valve. This can be clearly observed by comparing the distribution of the fluorescent dye in the valve and the absence of brightness at the edges of the membrane.

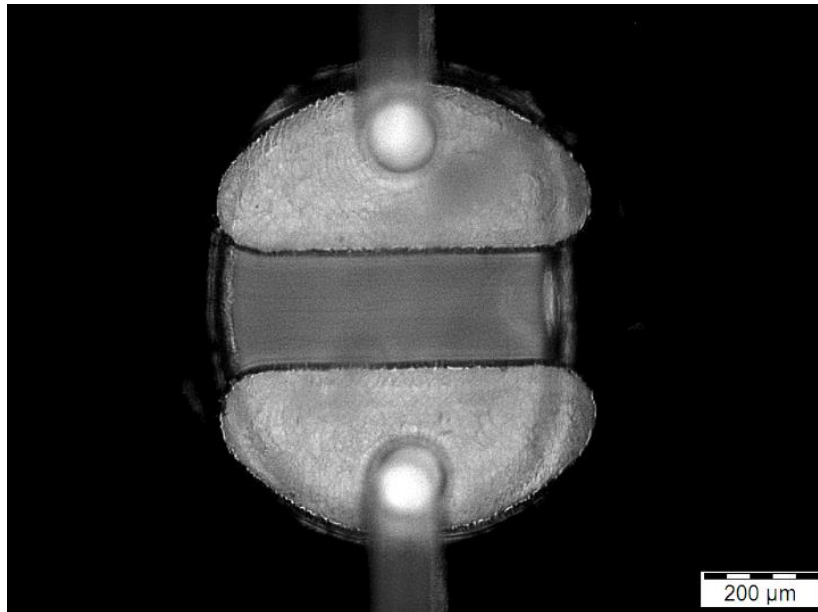


Figure 40. Membrane in plastic state, with presence of corrugations in the material

Another relevant result is presented in Figure 41. The image refers to a working valve part of a chip coming from the third batch of production. In this case, the amount of fluorescent dye present inside the valve is comparable to the previous results, but the area is much larger. This is caused by imperfection during the bonding process causing partial detachment and non-perfect bonding at the edges of the membrane, allowing the dye to accumulate at outer spots. This can be assessed noting in the picture the presence of an accumulation of dye on the perimeter of the valve

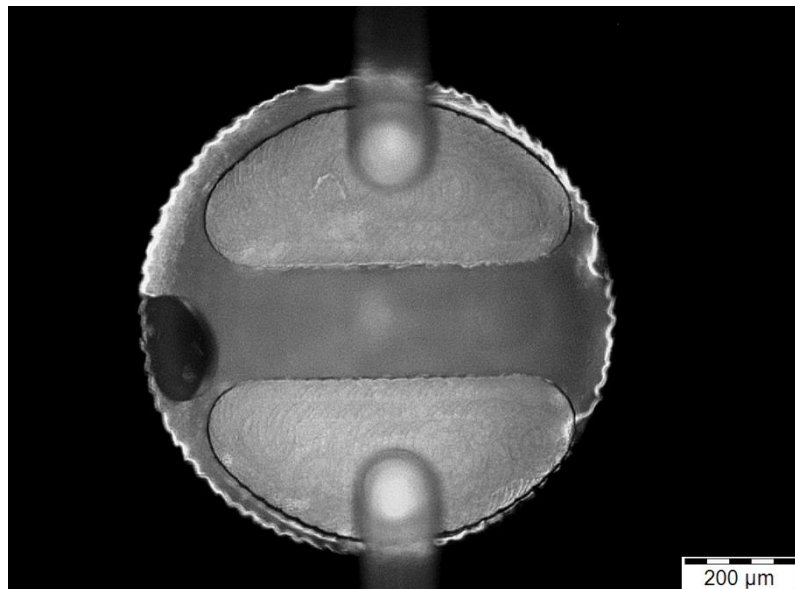


Figure 41. Fully functional valve with imperfect bonding at the edge of the membrane

Results of 3D and spatial analysis for valve characterization

In order to try to obtain a spatial representation of the membrane in a valve, the software was used to analyse the brightness of the pixels to obtain a 2D and a 3d representation.

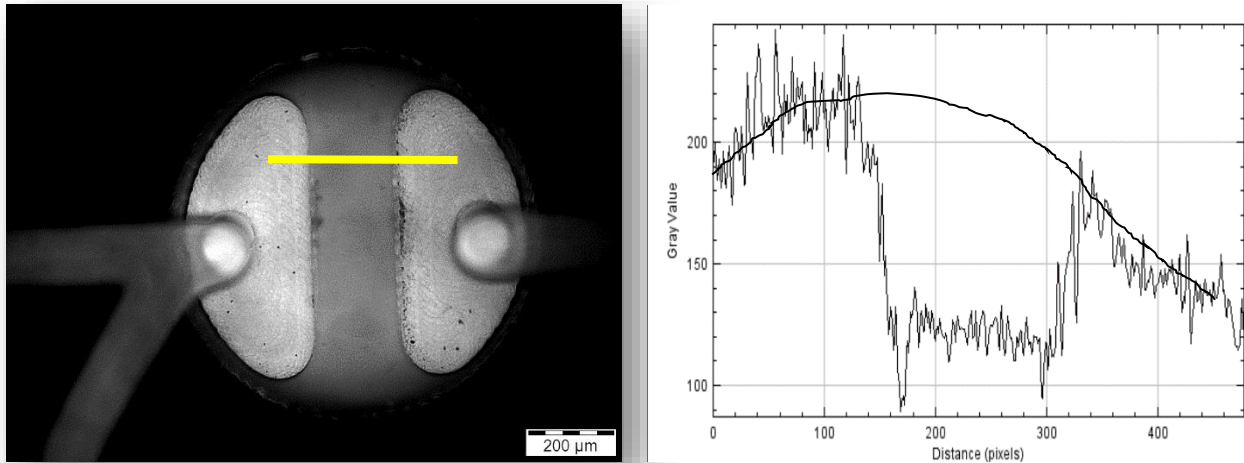


Figure 42. Use of the ImageJ software for the 2D analysis of the behavior of a membrane. The brightness of the pixels is extracted along a path (in yellow) and plotted

First the software was used to obtain a 2D representation of the membrane, and the results can be seen in Figure 42. A path is chosen on the image that is analysed, and the brightness of the pixels along that path is plotted on a graph. A curve representing the membrane can be interpolated from the graph and is presented in Figure 42. From the distance 0 to around 180 pixels the brightness of the liquid is high, and a curve can be extracted rising towards the centre of the valve. The same happens for the distance from 300 pixels to the end of the path, but the brightness in this case is lower due to the fact that the amount of liquid in the right part of the valve is lower. This is caused by the difference in pressure between the two parts of the valves, caused by the fluidic pressure of the liquid that is applied from left to right. Between 180 pixels and 300 pixels, the brightness is lower due to the geometry of the valve: Due to this, it is more difficult to extract the geometry of the valve from the middle segment and the middle segment is obtained with the connection of the left and right interpolation. The result shows a valve that has a cuspid shape in idle state and is a bit more deformed on the side directly exposed to the flow of the liquid.

To obtain a 3D representation of the liquid in the valve based on the brightness of the pixels the ImageJ 3D plug in was used. The results can be observed in Figure 43.

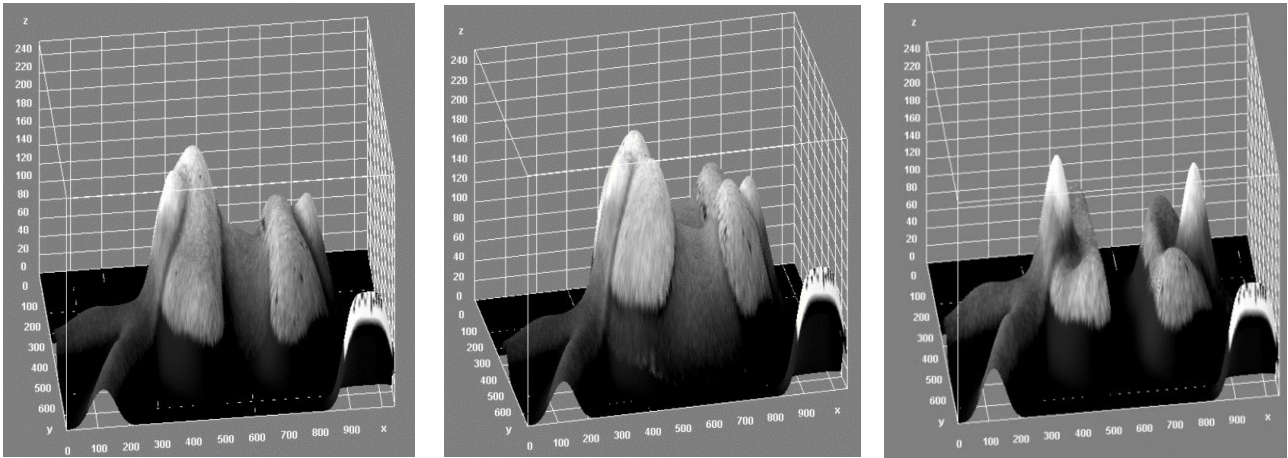


Figure 43. Results of 3D visualization based on the analysis of the brightness of the pixels. A) Valve in idle state. B) Valve in open state. C) Valve in closed state

The results can give an idea of the behaviour of the membrane and show differences between the membrane in the different actuation state. However, even if the tool and the results are both interesting and can be useful to compare the behaviour of the valves from the different batches of chips, is still difficult to exploit and obtain comparable data between the different set of valves. After the initial tests, it was decided that the fluorescence method was to be optimized and applied in future applications and study. For now, the results and the parameters explained can efficiently be used only for the comparison of the behaviour of the valve and the 2D analysis.

6.3. Characterization procedure

The following step in the characterization process was to test the flow rate and the flow stability inside the microfluidic chip during the pumping sessions. Chips from the 3 batches were tested to see the amount of consistency between the results and identify the impact of the change of production parameters on the performances of the chip. Unfortunately, of the three produced batches of chips, only the first two batches were found to be functional, while the last batch had a yield of 0 % on 8 samples. The results that are highlighted in the following paragraphs come from the experimental results of the tests performed on the first two batches of chip.

Flow rate testing

The first characterization test involved the quantification of the flow of liquid inside the microfluidic chip during a defined amount of time. The systems were tested at five different pump actuation speed, 50, 75, 100, 125 and 150 cycles per minutes (the cycle being the complete actuation cycle of the internal pump as it was defined in the previous chapter). The behavior of the pump was characterized by changing 2 different parameters, the actuation level and the actuation rate of the pump, both controlled through the software interface of the external pumping system. The actuation level is a percentage value describing the performances of the external pump; at an actuation level of 0% the pumping system is set off while at 100% the pumping system is at full power capacity. There is no much difference between actuation levels above 20 % as the machine produces results that are not significantly variable from the ones at a 20 % actuation. The flow rate is measured on the prototype chip and 2 chips coming from batch #2, which had 25% yield. Figure 44 shows the results of the measurement, in terms of average and dispersion. The flow rate is relatively consistent among the different chips for pumping rates below 100 cycles/minutes but became less homogeneous for rates above 100 cycles/minutes. This discrepancy was not analyzed in depth, but the cause was hypothesized to be related to clipping phenomena appearing in the valves when the actuation rate goes above a certain threshold. This phenomenon can change the average amount of liquid present inside the chamber when the actuation rate surpasses 100 cycle/minute, producing these alterations from the samples. The results were considered acceptable also because the standard actuation rate of the working system is 100 cycles/minutes, and the dispersion for this value among the different samples is extremely low.

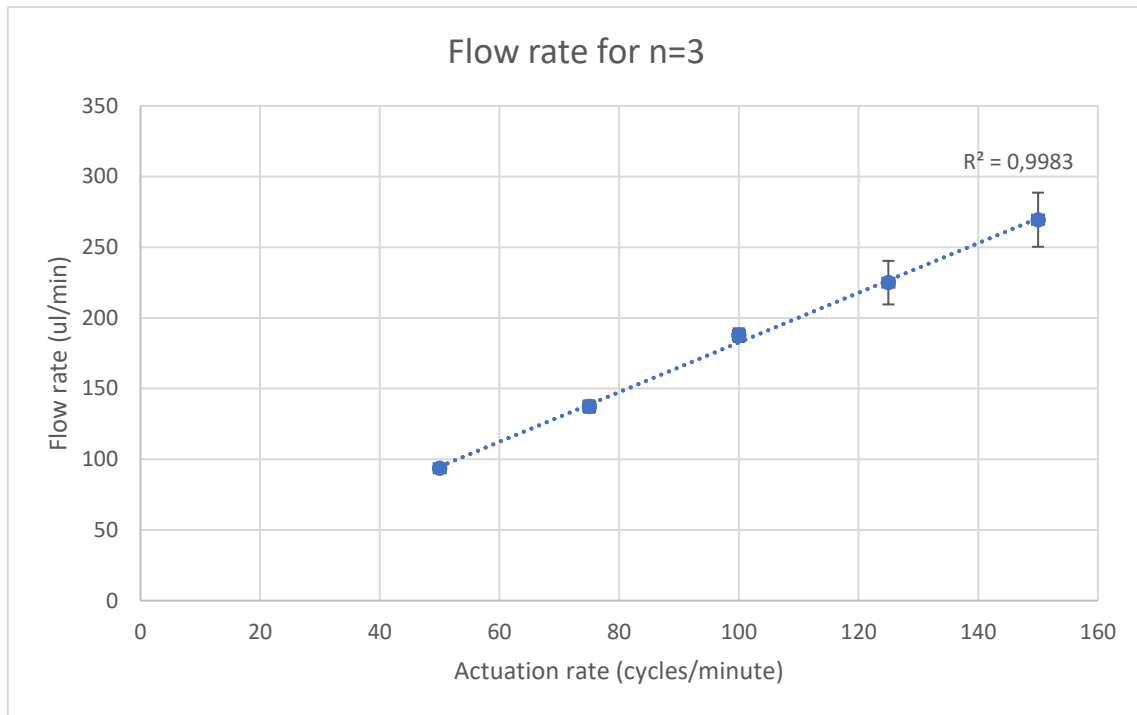


Figure 44. Flow rate characterization for the three analyzed chips

The second characterization procedure involved the analysis of the stability of the flow among the different samples. This was assessed by measuring the time interval necessary to pump intervals of 100 ml from 0 to 500 ml. This test was performed to observe if the system would change the amount of liquid pumped in a cycle depending on the amount of liquid already pumped during the process. The flow stability of the three samples was tested at 5 different flow rates, 50, 75, 100, 125 and 150 cycle/minute. Figure 45 shows the results of the characterization in terms of average and dispersion. For each flow rate, the curve describing the flow is linear, confirming the stability of the pump in the flowing process. The dispersion of the values increases with the amount of liquid pumped and it was hypothesized that the higher dispersion at higher volumes of pumped liquid was due to the accumulations of error measurements along the consecutive time intervals.

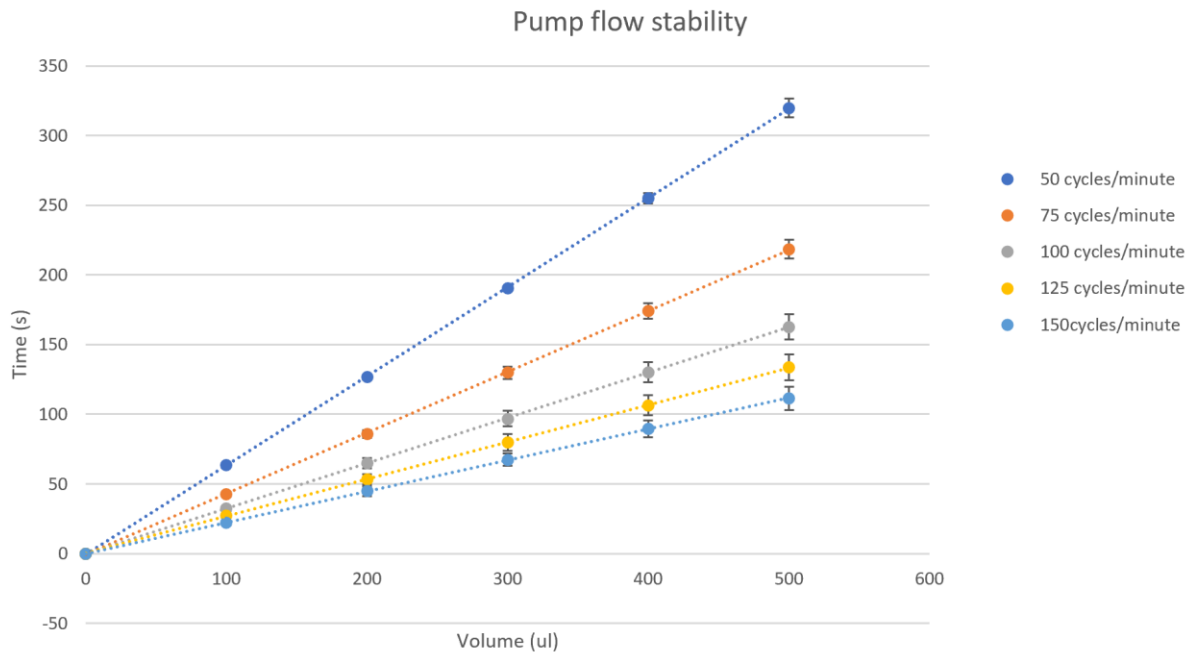


Figure 45. Flow stability characterization for the three analyzed chips

6.4. Magnetic nanoparticles testing

The following tests were performed to understand if the current microfluidic network is compatible with the MNP that will be used during the normal functioning of the device. The aim was to observe the behaviour of the MNPs in the microfluidic chip and the eventual presence of clogging in the fluidic channels or malfunctioning in the working routine of the microvalves. A solution of 200 nm amino-dextran MNPs at 0.02% solid content in PBS have been provided by UCBL to carry this test. A reservoir has been filled with 500 μL of this solution and pumped to the waste at an actuation rate of 100 cycles/min. This step has been repeated 8 times to process a total volume of 4 mL, which corresponds to the maximum volume with MNPs that the LOC is expected to process. The flow stability has been characterized similarly as is described in the previous steps and is compared to the one when pumping a solution of PBS without MNPs (Figure 46).

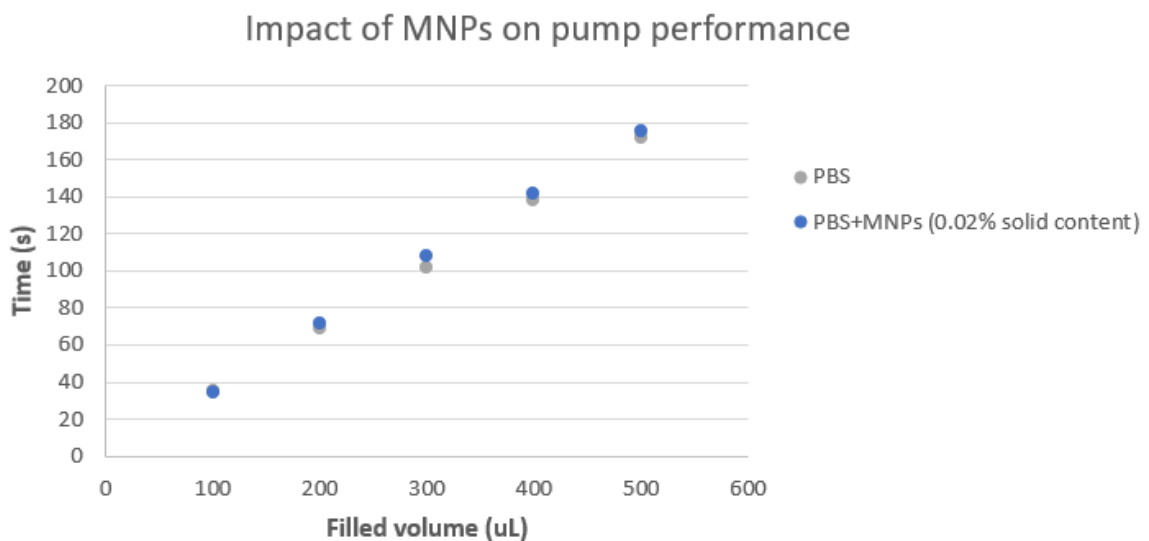


Figure 46. Characterization of the flow stability with and without MNPs.

The data shows no clear evidence of an impact of the MNPs on the flow rate achieved by the pump: similar filling rates are achieved disregarding the presence or not of MNPs in the solution pumped. A final check has been made by looking at the pump valves under a microscope to observe for a potential agglomeration of MNPs. Figure 47 shows the state of the pump valves when initiating the pumping of the solution with MNPs (Figure 47.A) and after pumping 4 mL of that solution (Figure 47.B).

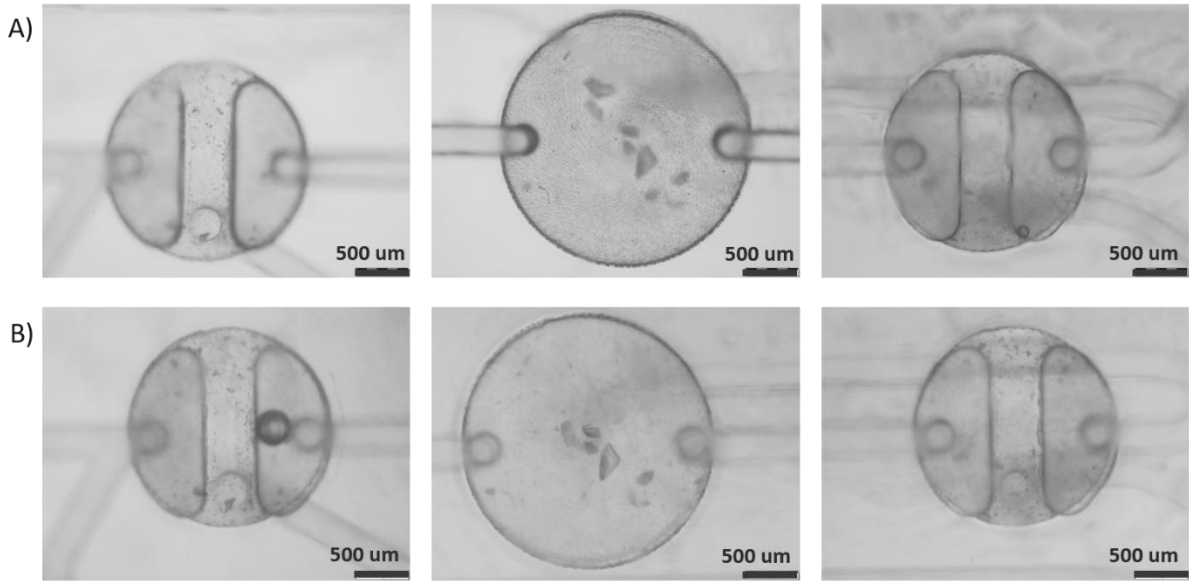


Figure 47. Microscope images of the micropump valves when pumping the MNPs solution from a sample reservoir to the waste reservoir. A) Pictures of each pump valves once the MNPs solution has just passed the micropump. B) Pictures of each pump valves after pumping 4 mL of the MNPs solution.

The results shown that there is no visible accumulation of particles or clumps confirming that the microfluidic networks prototyped is adequate to process such a solution incorporating MNPs.

6.5. Testing of the working assay

This paragraph presents the next step in the characterization process, consisting in the testing of the full behaviour routine of the chip. In order to proceed, a fully functional chip from the second batch of fabricated chips was used. Both the ISFET and the EM chamber were sealed by bonding pieces of glass slides using NOA68 glue, with the parameters obtained from the previous bonding experiment. All the reservoirs were filled with water dyed with a different colour, the buffer being deep blue and the samples red, yellow, green and orange.

The aim of this test was to observe the behaviour of the liquid during a complete working session, assess the presence and the amount of air bubbles in the channels and confirm that the tested sequence was optimal to obtain the desired output.

The full sequence was composed by 20 different steps, each one with a 25 seconds duration, for a total time of 8 minutes 20 second. Each step is described in the following paragraphs and the visual results obtained after each step are presented in the figures.

Step 1: Priming of the system with buffer (blue-stained PBS)

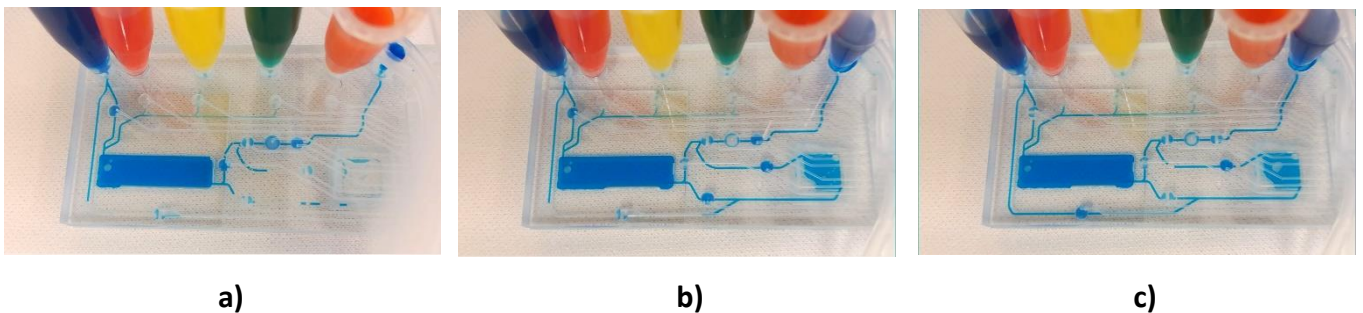


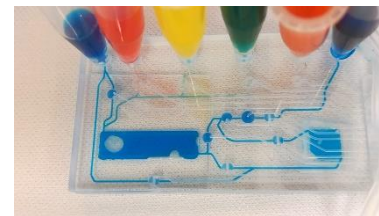
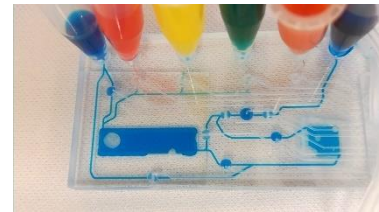
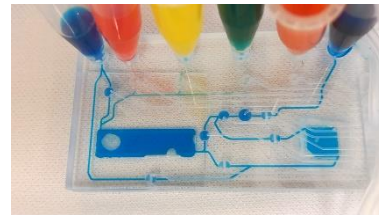
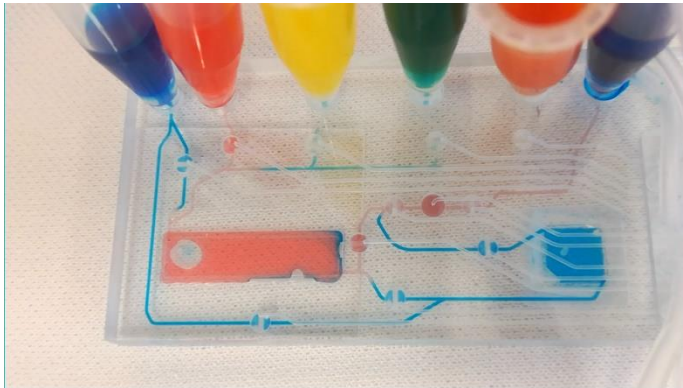
Figure 48. **a)** Filling of the magnetic chamber; **b)** Filling of the ISFET chamber through the magnetic chamber; **c)** Filling of the buffer to ISFET chamber line.

This first step primes the system and fills all the chambers and channels with the buffer. The sequence works as the buffer fills the system, but air bubbles are present both in the ISFET and in the EM chamber. The priming sequence will be further optimized during future test to minimize the presence of air bubble in the systems.

Step 2: Sample 1 processing

In this step the first sample is processed: First the sample is pumped through the EM chamber and then the buffer is employed to wash the magnetic nanoparticles from the EM chamber, to transfer

the magnetic nanoparticles from the EM chamber to the ISFET chamber and then used to remove the MNPs from the EM chamber cleaning it.



a)

Figure 49. sample 1 processing

- a) EM Chamber filling
- b) EM chamber wash (MNPs wash)
- c) Transfer from the EM chamber to ISFET chamber
- d) EM chamber cleaning (MNPs removal)

The main problem of this step is that the air bubble present in the EM chamber increased in size, due to the pumping of the air present between the inlet and the valve connecting the sample tanks and the EM chamber.

Step 3: Sample 2 processing

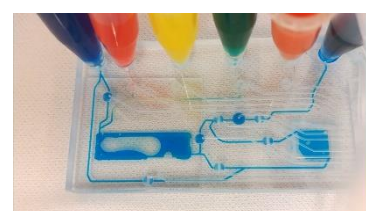
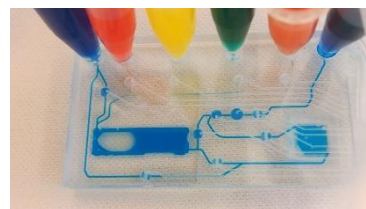
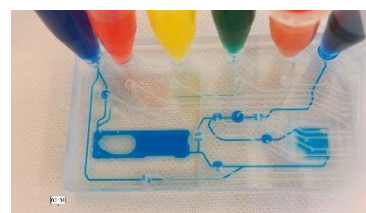
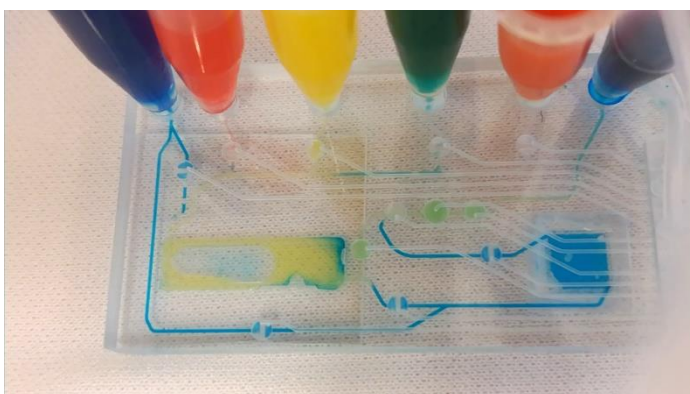


Figure 50. sample 2 processing

- a) EM Chamber filling
- b) EM chamber wash (MNPs wash)
- c) Transfer from the EM chamber to ISFET chamber
- d) EM chamber cleaning (MNPs removal)

In this step the second sample is processed. The sequence is the same as step 2. The air bubble present in the EM chamber increased in volume and extension.

Step 4: Sample 3 processing

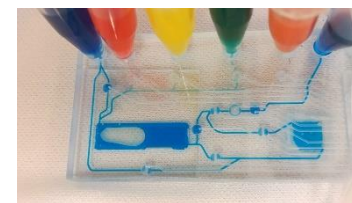
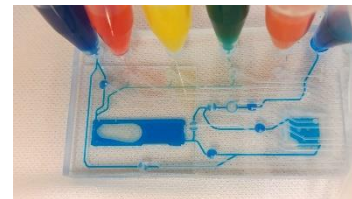
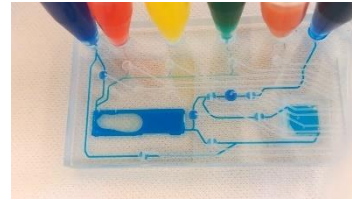
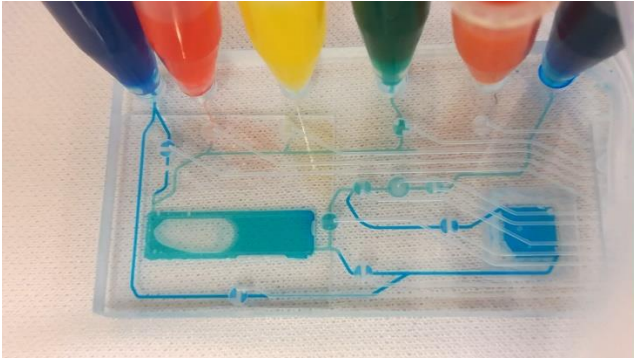


Figure 51. Sample 3 processing

- a) EM Chamber filling
- b) EM chamber wash (MNPs wash)
- c) Transfer from the EM chamber to ISFET chamber
- d) EM chamber cleaning (MNPs removal)

In this step the sample 3 is processed. The sequence is the same as step 2. The air bubble present in the EM chamber remained around the same extension and volume as in step 3.

Step 5: Sample 4 processing

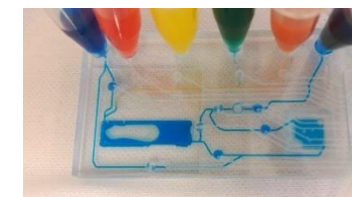
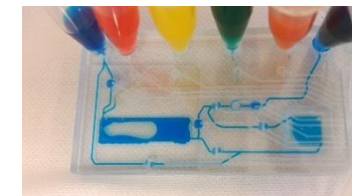
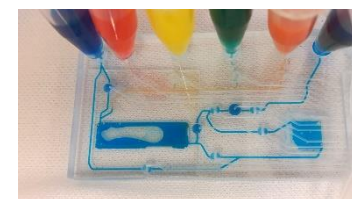
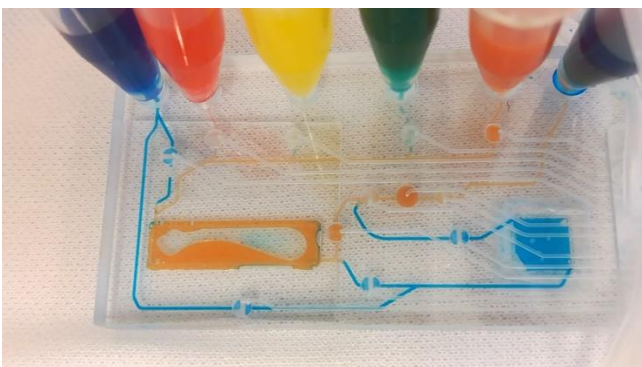


Figure 52. sample 4 processing

- a) EM Chamber filling
- b) EM chamber wash (MNPs wash)
- c) Transfer from the EM chamber to ISFET chamber
- d) EM chamber cleaning (MNPs removal)

In this step the last sample, sample 4, is processed. The sequence is the same as the previous steps. The air bubble present in the EM chamber remained around the same volume but changed in extension, occupying nearly all the EM chamber.

Step 6: ISFET chamber washing

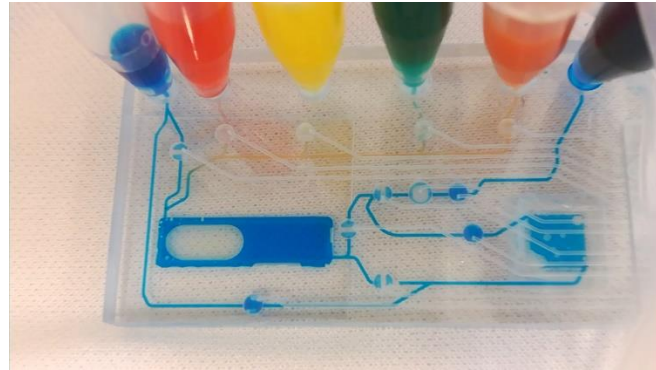


Figure 53. Buffer flowing to the waste without passing through the magnetic chamber

This is the last step and consists in the washing of the ISFET chamber. For all the routine of the chip the disposition and the amount of air bubble present in the ISFET chamber increased slightly, creating clusters of air in the two main chambers that can be disruptive during a complete work session of the microfluidic chip. In order to reduce the amount of air present in the microfluidic chip during the normal working routine, a priming sequence was developed and tested.

6.6. Priming optimization

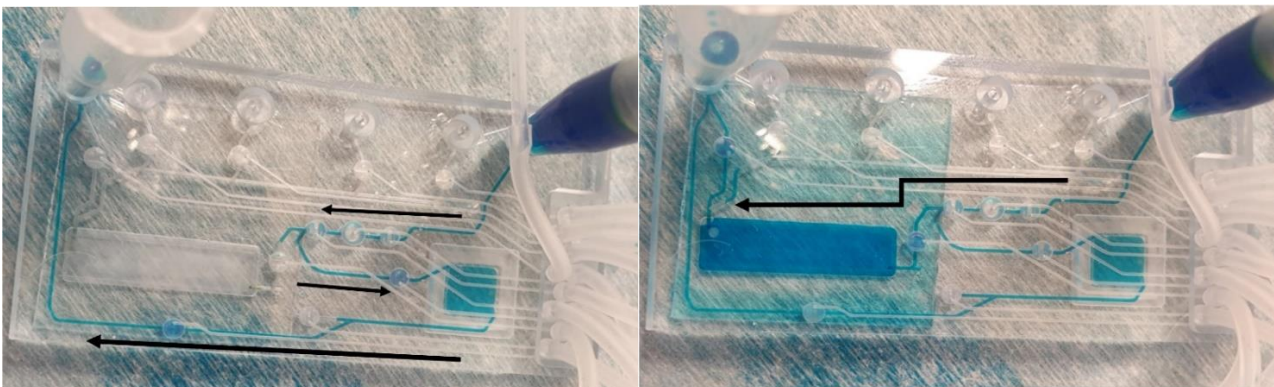
After the testing of the complete working sequence of the chip, the following step was to optimize the priming sequence. The aim of this section of the work was to identify a configuration of action suitable to prime the system and eliminate all the air present in the chambers and in the channels of the chip in order to avoid the formation of bubbles during the actuation period of the chip. Different set of operation were tested on 3 chips that were functional from the second batch and whose chambers were covered by glass slides glued through the use of NOA 68 glue. The tests were made alternating the direction of the flow, backwards from the waste tank to the buffer and sample tanks and forward from the buffer and samples tank to the waste tank.

Identified problems to overcome

During the test done on the second batch of chip the bubble formation and air presence inside the channels was confirmed to be a problem. The initial priming step consisted in the pumping of the buffer along the channels of the whole chip towards the waste. This step was confirmed to be insufficient to eliminate the presence of air, since the air present between the sample tanks and the line connecting the buffer to the waste was impossible to eliminate. In this framework, it was fundamental to find a new way to prime the system. One of the options that was taken into consideration was to flow back a small, uninfluential amount of buffer from the buffer tank towards the sample tank to push the air stuck in the inlets through the sample tanks. The next tests were performed to individuate a sequence of steps to incorporate this new action in the priming process.

First test methodology and priming result

The next step in the characterization of the microfluidic chip was to observe the behaviour of the liquid in the two chambers when the chambers are sealed by a rigid material and not by an adhesive layer. The ISFET chamber was sealed by a COC chip, being slightly hydrophobic, while the magnetic chamber was sealed by a piece of glass slides. The first results were good, and a better flow conformity is achieved. Unfortunately, some bubbles were still present inside the chamber and were impossible to remove at the different cycle rate. Different flow conditions were tried, both at low and high pumping rate, but at the end of the process there was still some amount of air left inside the two main chambers.



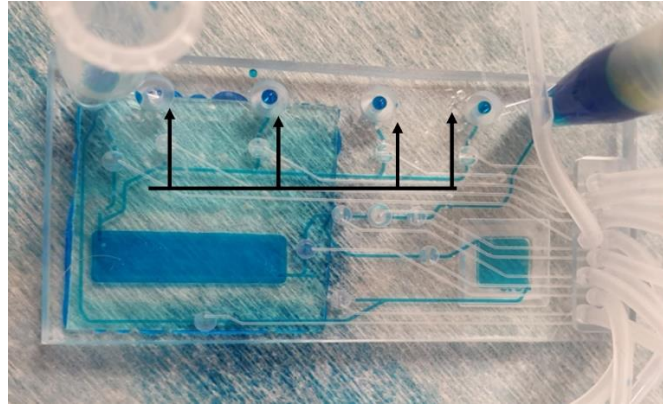


Figure 54. Testing of the backflow sequence for the priming of the system. A) Buffer is pumped from the waste tank to the buffer tank through the ISFET chamber. B) Buffer is pumped through the magnetic chamber. C) Buffer is pumped through the tanks outlet

Figure 54 shows the configuration in which the chambers of the microfluidic chip are sealed by COC slides. In this configuration, the liquid tanks were not connected to the chip and the buffer tank was left empty while the waste tank was filled with PBS. The first step in the sequence consisted in the backfilling of both the ISFET and the EM chamber and the pump actuated a backward flow from the waste tank to the buffer tank at a rate of 50 cycles/minute. The flow rate chosen was the slowest available one to observe better the behaviour of the liquid inside the channels and the chambers. The results of this step were promising, and the filling of both chambers was nearly uniform, but still a small bubble of air in the top left corner of the magnetic chamber was present. The following step consisted in the filing of the reservoir line, pumping the air present in the connecting line towards the external environment. The valves sealing the different sample tanks were opened sequentially and the air was successfully pumped out of the channels by the fluid flowing backward from the waste tank. The third step in this sequence consisted in the filling of the line connecting the buffer tank to the ISFET chamber. The priming was consistent, but we observed a small bubble of air that remained stuck at the buffer reservoir inlet. The last step consisted in eliminate the air present in the chip between the two chambers. Valves 5 and 8 were opened and the air was successfully eliminated from the system this time pumping the liquid forward. Figure 54 shows the result obtained with the application of this sequence.

Second test methodology and results

For this second test the sequence was changed to see how the results differed from the previous ones. The set up for this sequence was identical to the set up employed in the first test. The first step in this sequence consisted in the filling of the channel connecting the buffer tank and the ISFET

chamber, followed by the filling of both chambers. Both steps were done employing a backward flow, and the results obtained were superior to the ones obtained in the previous experiment. The chambers were filled almost perfectly, except for the presence of small bubbles of air at the inlet of the EM chamber. The third step in the sequence was identical to the third step in the first experiment, in which the valves connecting the EM chambers and the tanks were opened sequentially and the fluid was pumped backwards from the waste to the tank. The achieved filling was uniform in this configuration. The final step consisted in the filling of the space between the two chambers. This step was unsuccessful as the air present near valve #7 was pushed into the ISFET chamber and was impossible to move. To avoid this problem in the future, it was decided that one step at the beginning of the sequence would have consisted in a flow from valve 7 to the EM chamber. Figure 55 presents the results of this unsuccessful priming attempt



Figure 55. Unsuccessful priming attempt, with internal bubbles still present

Future test on the priming sequence will include functionalized surfaces sealing the different chambers to assess if the change in chemical properties of the liquid path influence the amount of air trapped inside the chip.

7. Conclusions and next steps

This final chapter summarizes the work performed during the internship and introduces the next steps to be performed in the KardiaTool project. The first part of the work revolved around the integration of the two silicon sensors in the microfluidic chip. In order to obtain data and test the different glues in order to find the optimal one, four kinds of different glues were dispensed with different parameters on the walls of a mock-up chip fabricated on the design of the final microfluidic chip. The optimization of the different parameters led to a deposition of glue with good localization on the inner walls of the microfluidic chamber. The important result at this step of the localization of the glue, with none to minimum overflow after the contact with a glass slide used for the testing purpose. The hermeticity and the resistance of the bonding to pressure and liquid flow was tested through the application of positive pressure and fluorescence liquid, and all the different glues were found able to generate a hermetic bonding. The next step of the process regarding the sensor integration consists in the repetition of the bonding tests with sealing materials with surface energies different from the surface energy of the glass. Materials like Si_3N_4 and HfO_2 that are possible options for the functionalization of the inner chambers will be tested and the dispensing results will be compared to the ones obtained to the one found with the glass cover, in terms of uniformity of deposition and bonding strength. The following step will consist in the change of the design of the testing chip, observing how the modification of the geometry of the channels, valve and the inner chambers will impact on the flow of the liquid and the performances of the microfluidic chip. The bonding obtained with these new designs of chip will also need to be tested in a more stable configuration, with the microfluidic chip fixed to the PCB through filler glue.

The second part of the work revolved around the characterization of the fluidic behaviour of the microfluidic chip from different batches in terms of characterization of the flow of the liquid and of the microfluidic valves and the testing of the working assay for the microfluidic chip. The results obtained with the tests were communicated to the team responsible for the fabrication of the chips for an iterative process aimed to the improving of the parameters for the fabrication of microfluidic chips. For the future, the next steps regarding the characterization of the polymeric cartridges will involve the testing and the characterization of the new design of the microfluidic chip obtained with the optimized bonding parameters. Once the new chips are characterized and found to be fully functional, the behaviour of the polymeric cartridge will be characterized while integrated in the

working KardiaTool platform. Another step that is not fundamental but can be interesting for the characterization of the microfluidic chip would be to find a process to characterize analytically and in a determined way the behaviour of the integrated valves through fluorescence microscopy.

8. Bibliography

- [1] C. F. O. R. Nanotechnologies, "KardiaTool platform proposal," 2016.
- [2] Eurostat, "Cardiovascular diseases statistics - eurostat," *Eurostat Stat. Explain.*, no. October 2015, p. 14, 2018.
- [3] W. Lesyuk, C. Kriza, and P. Kolominsky-Rabas, "Cost-of-illness studies in heart failure: A systematic review 2004-2016," *BMC Cardiovasc. Disord.*, vol. 18, no. 1, pp. 1–11, 2018.
- [4] U. E. Clare Taylor, Primary Care Clinical Sciences, School of Health and Population Sciences, Primary Care Clinical Sciences Building, University of Birmingham, B15 2TT, "Diagnosing Heart Failure-Experience and 'Best Parhways,'" *Eur. Cardiol.*, vol. 6, no. 3, pp. 10–12, 2010.
- [5] E. E. Tripoliti, T. G. Papadopoulos, G. S. Karanasiou, K. K. Naka, and D. I. Fotiadis, "Heart Failure: Diagnosis, Severity Estimation and Prediction of Adverse Events Through Machine Learning Techniques," *Comput. Struct. Biotechnol. J.*, vol. 15, pp. 26–47, 2017.
- [6] N. E. Ibrahim and J. L. Januzzi, "Established and emerging roles of biomarkers in heart failure," *Circ. Res.*, vol. 123, no. 5, pp. 614–629, 2018.
- [7] K. S. Singh P, Gupta ND, Bey A, "Salivary TNF-alpha: A potential marker of periodontal destruction," *indian Soc Periodontol.*, vol. 18, no. 3, pp. 306–10, 2014.
- [8] J. Y. Y. Foo *et al.*, "NT-ProBNP Levels in Saliva and Its Clinical Relevance to Heart Failure," *PLoS One*, vol. 7, no. 10, pp. 1–6, 2012.
- [9] R. L. Dekker *et al.*, "Salivary Biomarkers, Oral Inflammation, and Functional Status in Patients With Heart Failure," *Biol. Res. Nurs.*, vol. 19, no. 2, pp. 153–161, 2017.
- [10] K. An, J. Salyer, R. E. Brown, H. F. S. Kao, A. Starkweather, and I. Shim, "Salivary Biomarkers of Chronic Psychosocial Stress and CVD Risks: A Systematic Review," *Biol. Res. Nurs.*, vol. 18, no. 3, pp. 241–263, 2015.
- [11] S. Amur, "Biomarker Qualification Program Educational Module Series-Module 1 Biomarker Terminology: Speaking the Same Language."
- [12] V. L. Roger, "Failure : a community study," *Heal. (San Fr.)*, vol. 118, no. 6, pp. 625–631, 2009.
- [13] C. Zhang *et al.*, "Saliva in the diagnosis of diseases," *Nat. Publ. Gr.*, no. 14, pp. 133–137,

2016.

- [14] B. Michalke, B. Rossbach, T. Göen, A. Schäferhenrich, and G. Scherer, "Saliva as a matrix for human biomonitoring in occupational and environmental medicine," *Int. Arch. Occup. Environ. Health*, vol. 88, no. 1, pp. 1–44, 2014.
- [15] Analytical Methods Committee, "AMC Technical Briefs 37 - Standard additions: myth and reality," *R. Soc. Chem.*, p. 2, 2009.
- [16] A. K. Au, H. Lai, B. R. Utela, and A. Folch, *Microvalves and micropumps for BioMEMS*, vol. 2, no. 2. 2011.
- [17] R. Mohan, B. R. Schudel, A. V. Desai, J. D. Yearsley, C. A. Apblett, and P. J. A. Kenis, "Design considerations for elastomeric normally closed microfluidic valves," *Sensors Actuators, B Chem.*, vol. 160, no. 1, pp. 1216–1223, 2011.
- [18] A. Manuscript, "Cell handling using microstructured membranes," *Bone*, vol. 23, no. 1, pp. 1–7, 2008.
- [19] R. G. Blazej, P. Kumaresan, and R. A. Mathies, "Microfabricated bioprocessor for integrated nanoliter-scale Sanger DNA sequencing," *Proc. Natl. Acad. Sci.*, vol. 103, no. 19, pp. 7240–7245, 2006.
- [20] Y. S. Lee, N. Bhattacharjee, and A. Folch, "3D-printed Quake-style microvalves and micropumps," *Lab Chip*, vol. 18, no. 8, pp. 1207–1214, 2018.
- [21] M. A. Unger, M. A. Unger, H. Chou, T. Thorsen, A. Scherer, and S. R. Quake, "Monolithic Microfabricated Valves and Pumps by Multilayer Soft Lithography," *Science*, vol. 113, no. 2000, pp. 113–116, 2013.
- [22] W. H. Grover, R. H. C. Ivester, E. C. Jensen, and R. A. Mathies, "Development and multiplexed control of latching pneumatic valves using microfluidic logical structures," *Lab Chip*, vol. 6, no. 5, pp. 623–631, 2006.
- [23] T. K. Indira and P. K. Lakshmi, "Magnetic nenoparticles-A review," vol. 3, no. 3, 2010.
- [24] J. Kudr *et al.*, "Magnetic Nanoparticles: From Design and Synthesis to Real World Applications," *Nanomaterials*, vol. 7, no. 9, p. 243, 2017.
- [25] A. Akbarzadeh, M. Samiei, and S. Davaran, "Magnetic nanoparticles: Preparation, physical

properties, and applications in biomedicine,” *Nanoscale Res. Lett.*, vol. 7, no. 1, p. 144, 2012.

- [26] P. B. Lippa, L. J. Sokoll, and D. W. Chan, “Immunosensors - Principles and applications to clinical chemistry,” *Clin. Chim. Acta*, vol. 314, no. 1–2, pp. 1–26, 2001.
- [27] S. Mehrabani, A. J. Maker, and A. M. Armani, “Hybrid integrated label-free chemical and biological sensors,” *Sensors (Switzerland)*, vol. 14, no. 4, pp. 5890–5928, 2014.
- [28] C. S. Lee, S. Kyu Kim, and M. Kim, “Ion-sensitive field-effect transistor for biological sensing,” *Sensors*, vol. 9, no. 9, pp. 7111–7131, 2009.
- [29] J. Chen and J. Liou, “On-chip spiral inductors for RF applications: an overview,” *J. Semicond. Technol. Sci.*, vol. 4, no. 3, pp. 149–167, 2004.
- [30] I. Burdallo, C. Jimenez-Jorquera, C. Fernández-Sánchez, and A. Baldi, “Integration of microelectronic chips in microfluidic systems on printed circuit board,” *J. Micromechanics Microengineering*, vol. 22, no. 10, 2012.
- [31] T. Brettschneider, C. Dorrer, M. Bründel, R. Zengerle, and M. Daub, “Wafer-level packaging and laser bonding as an approach for silicon-into-lab-on-chip integration,” *J. Micromechanics Microengineering*, vol. 23, no. 5, 2013.
- [32] C. Lu, L. J. Lee, and Y. J. Juang, “Packaging of microfluidic chips via interstitial bonding technique,” *Electrophoresis*, vol. 29, no. 7, pp. 1407–1414, 2008.
- [33] L. Zhu, D. Meier, Z. Boger, C. Montgomery, S. Semancik, and D. L. DeVoe, “Integrated microfluidic gas sensor for detection of volatile organic compounds in water,” *Sensors Actuators, B Chem.*, vol. 121, no. 2, pp. 679–688, 2007.
- [34] “DD-500 device user manual.”
- [35] “NORLAND PRODUCTS INCORPORATED Norland Optical Adhesive 68,” 1966.
- [36] M. D. Adhesives, “MD[®] MEDICAL DEVICE ADHESIVES 1072-M Product Data Sheet Non-Fluorescing , Flexible Plastics Adhesive MD[®] MEDICAL DEVICE ADHESIVES 1072-M Product Data Sheet.”
- [37] H. Strength and T. C. Properties, “PERMABOND[®] UV632 UV-Curable Adhesive Technical Datasheet Features & Benefits Cure on demand High shear strength Fast curing with low-

power lamps Typical Performance of Cured Adhesive Physical Properties of Uncured Adhesive Storage & Handling," no. June, pp. 1–2, 2018.

[38] P. Description *et al.*, "IQ-BOND 8419 UV," vol. 6, pp. 3–4, 2016.